

See discussions, stats, and author profiles for this publication at: <https://www.researchgate.net/publication/348590404>

Sequence stratigraphic and petrological analyses of the Cambrian oncoids exposed in the Liaoning Province, North China Platform

Article in *Australian Journal of Earth Sciences* · January 2021

DOI: 10.1080/08120099.2021.1858156

CITATIONS

3

READS

222

4 authors:



Enzhao Xiao

Polar Research Institute of China

30 PUBLICATIONS 132 CITATIONS

[SEE PROFILE](#)



Tehseen Zafar

Peking University

55 PUBLICATIONS 225 CITATIONS

[SEE PROFILE](#)



Muhammad Riaz

China University of Geosciences (Beijing)

44 PUBLICATIONS 185 CITATIONS

[SEE PROFILE](#)



Khalid Latif

University of Peshawar

69 PUBLICATIONS 196 CITATIONS

[SEE PROFILE](#)

Some of the authors of this publication are also working on these related projects:



Supported by OGDCL and University of the Punjab Lahore Pakistan [View project](#)



Application and extension of Geometric Factor Theory (GFT) on present day reservoirs [View project](#)



Australian Journal of Earth Sciences

An International Geoscience Journal of the Geological Society of Australia

ISSN: (Print) (Online) Journal homepage: <https://www.tandfonline.com/loi/taje20>

Sequence stratigraphic and petrological analyses of the Cambrian oncoids exposed in the Liaoning Province, North China Platform

E. Z. Xiao , S. Jiang , T. Zafar , M. Riaz , K. Latif , E. Setoyama , H. Wang & H. Xin

To cite this article: E. Z. Xiao , S. Jiang , T. Zafar , M. Riaz , K. Latif , E. Setoyama , H. Wang & H. Xin (2021): Sequence stratigraphic and petrological analyses of the Cambrian oncoids exposed in the Liaoning Province, North China Platform, Australian Journal of Earth Sciences, DOI: [10.1080/08120099.2021.1858156](https://doi.org/10.1080/08120099.2021.1858156)

To link to this article: <https://doi.org/10.1080/08120099.2021.1858156>



Published online: 18 Jan 2021.



Submit your article to this journal [↗](#)



View related articles [↗](#)



View Crossmark data [↗](#)

Sequence stratigraphic and petrological analyses of the Cambrian oncoids exposed in the Liaoning Province, North China Platform

E. Z. Xiao^a , S. Jiang^b, T. Zafar^c , M. Riaz^d , K. Latif^e , E. Setoyama^f, H. Wang^g and H. Xin^h

^aKey Laboratory for Polar Science, MNR, Polar Research Institute of China, Shanghai, China; ^bState Key Laboratory of Sedimentary Basin and Energy Resources & Faculty of Earth Resources, China University of Geosciences, Wuhan, China; ^cInstitute of Geochemistry, Chinese Academy of Sciences, Guiyang, China; ^dState Key Laboratory of Oil and Gas Reservoir Geology and Exploitation, Chengdu University of Technology, Chengdu, China; ^eCollege of Energy Resources, Chengdu University of Technology, Chengdu, China; ^fNational Centre of Excellence in Geology, University of Peshawar, Peshawar, Pakistan; ^gEnergy & Geoscience Institute (EGI), University of Utah, Salt Lake City, UT, USA; ^hSchool of Earth Sciences and Resources, China University of Geosciences, Beijing, China

ABSTRACT

The Cambrian Miaolingian Series strata are continuously exposed in the North China Platform and contain diverse sedimentary phenomena, including substantial with oncoid-rich units. Limestone samples from the Zhangxia Formation in the Sandaogou section were collected to characterise unique macroscale to microscale sedimentary characteristics of the marine carbonate oncoids. In the oncolitic beds (~4.5 m thick), the individual size of oncoids gradually increases from bottom to top. The oncoid morphology and the presence of a nucleus and laminae in thin-sections are used to classify these oncoids into three types (concentric laminar, lateral growth and multicore oncoids). As evidenced by scanning electron microscopy and energy-dispersive X-ray observations, *Girvanella* are abundant inside these oncoids and are associated with nanospheres, framboidal pyrite, and spherical and filamentous microbial fossils, confirming the biogenicity of the studied oncoids. These results suggest that the oncolitic–oolitic limestone formed in an upward-shallowing marine environment caused by a forced regression process that resulted in a decrease in accommodation space in a fourth-order sequence. Thus, the conditions became increasingly suitable for the development of cyanobacteria-dominated microbial mats and large oncoids. The late stage of the depositional setting and elevated solar radiation resulted in the formation of the growth termination surface.

KEY POINTS

1. Evidence of microbial origin from the oncoids of the Cambrian Miaolingian Series in the North China Platform.
2. Vertical variation in oncoid size and distribution coincide with geochemical data.
3. A shallowing depositional environment is interpreted as the reason for variation in oncoid size and formation of oncoid growth termination surfaces.

ARTICLE HISTORY

Received 3 November 2019
Accepted 26 November 2020

KEYWORDS

sequence stratigraphy; oncoids; *Girvanella*; microbial mat; Zhangxia Formation; Miaolingian

Introduction

After the global extinction event of archaeocyaths at the end of the Cambrian Epoch 2 (Kiessling, 2009; Xiao *et al.*, 2018), deposition of the Miaolingian Series on the North China carbonate platform was dominated by ooid shoals (Riaz, Xiao, *et al.*, 2019). This period is characterised by the termination of an anoxic event (Hough *et al.*, 2006; Zhang *et al.*, 2014), a rise in the global sea-level (Pratt & Bordonar, 2007; Pruss *et al.*, 2010) and an increase in metazoan abundance (Peng *et al.*, 2012). Based on the discovery of fossilised cyanobacteria and the abrupt increase in microbial carbonate, this period is considered the first episode of the cyanobacteria calcification event in the Phanerozoic and represents a period of microbialite recovery (Latif *et al.*,

2019; Riding, 2006; Riding & Liang, 2005; Xiao *et al.*, 2018). Large numbers of marine carbonate oncoids have been found in the Cambrian Miaolingian Series strata of the North China Platform (Han *et al.*, 2015; Wang & Xiao, 2018; Xiao, Mei, *et al.*, 2020; Xiao, Wang, *et al.*, 2020; Zhang *et al.*, 2014), and these deposits provide important insights into the origins of oncoids and their responses to paleoenvironmental factors.

Oncoids with nucleus-cortex structures are easily differentiated from other carbonate grains (Flügel & Munnecke, 2010; Tucker & Wright, 1990). In the majority of cases, oncoids are regarded as biogenic; however, owing to their diverse forming environments, there are different interpretations of their formation mechanisms (Hägele *et al.*, 2006; Han *et al.*, 2015; Jones & Renaut, 1997; Shapiro *et al.*, 2009;

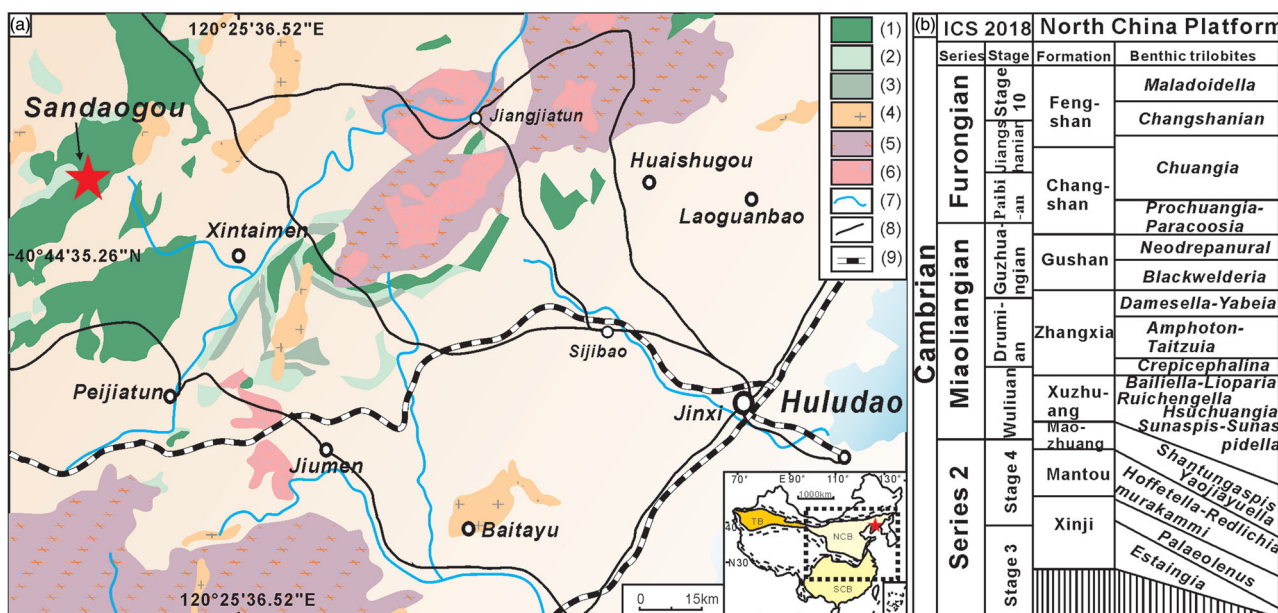


Figure 1. Geological setting of the study area. (a) Cambrian outcrops in the investigated area near Huludao city, Liaoning province in NE China (red star indicates the location of the Sandaogou section). 1, Cambrian outcrops; 2, Ordovician outcrops; 3, Carboniferous outcrops; 4, quartz monzonite; 5, trachyandesite porphyrite; 6, granite porphyry; 7, river; 8, highway; 9, railway. (b) Cambrian stratigraphic succession of the North China Platform and correlations with international chronostratigraphic subdivisions (Haq & Schutter, 2008; Peng *et al.*, 2012; Wang *et al.*, 2000).

Wang & Xiao, 2018; Yang *et al.*, 2011). To date, the research on the origin of oncoids is mostly based on the combined classification of morphology, mineral composition and environmental setting (Peryt, 1983; Védérine, 2008; Védérine *et al.*, 2007; Yang *et al.*, 2011; Zhang *et al.*, 2014; Zhou *et al.*, 2017). Marine carbonate oncoids have been interpreted to originate through the following processes: (1) microbially mediated calcium carbonate precipitation, (2) complex metabolic mechanisms within microbial communities (microbial mats) and (3) formation of laminae via by trapping and binding in a marine environment (Dahanayake, 1977; Flügel & Munnecke, 2010; Han *et al.*, 2015; Jones, 2011; Jones & Renaut, 2010; Peryt, 1983; Qi *et al.*, 2016; Wang & Xiao, 2018; Xiao, Mei, *et al.*, 2020; Xiao, Wang, *et al.*, 2020; Xiao, Zafar, *et al.*, 2020; Yang *et al.*, 2011; Zhang *et al.*, 2014; Zhang *et al.*, 2015). The genesis mechanisms of these oncoids are analogous to microbialites (Mei, 2007; Wang & Xiao, 2018). Oncoids are also defined as a variety of carbonate particles associated with microbial mat sediments (Gerdes *et al.*, 1994).

This study examines several types of well-preserved marine carbonate oncoids within oolitic limestones from the upper part of the Zhangxia Formation (Cambrian Miaolingian Series), which is exposed in the Sandaogou section of the North China Platform. Two significant macroscopic phenomena are observed: (1) in beds containing oncoids, the individual size of oncoids gradually increases from bottom to top; and (2) in the thin beds of oncoids, a distinct oncoid growth termination surface is observed (Figure 1). This study adopted petrological and geochemical methods, including scanning electron microscopy (SEM), energy-dispersive X-ray detection (EDX), X-ray

diffraction (XRD), and carbon and oxygen isotope data, to explore the formation mechanism and controlling factors of the Cambrian marine carbonate oncoids in the study area. The results show that sea-level change affected the cyanobacterial mats and the construction of oncoids. The depth of depositional environment affected the growth of cyanobacteria microbial mats, resulting in variations in the size of oncoids and the formation of growth termination surface.

Geological setting and sequence stratigraphic framework

The Sandaogou section is located 40 km to the northwest of the city of Huludao near the town of Xinmentai in Liaoning Province, North China Platform (Figure 1a). At the base of the Sandaogou section the sediments were deposited in an offshore marine environment (Feng *et al.*, 2004; Xiao, Mei, *et al.*, 2020). Under the new chronostratigraphic scheme (Fan *et al.*, 2015; Peng *et al.*, 2012; Xiao, Mei, *et al.*, 2020), the Cambrian Miaolingian Series strata exposed in the Sandaogou section comprise the Maozhuang, Xuzhuang, Zhangxia and Gushan formations (Figure 1; Latif *et al.*, 2018; Riaz, Xiao, *et al.*, 2019; Riaz, Latif, *et al.*, 2019; Xiao, Sui, *et al.*, 2017; Xiao, Qin, *et al.*, 2017). The Zhangxia Formation was deposited during the late Wuliuan to late Drumian stages (Peng *et al.*, 2012) (Figure 1b).

Internal lithological characteristics in the Zhangxia Formation display cyclic changes from nongrain bank facies to grain bank and deep-water facies to shallow-water facies, demonstrating several shallowing-upward cycles. The boundary between the Zhangxia and underlying

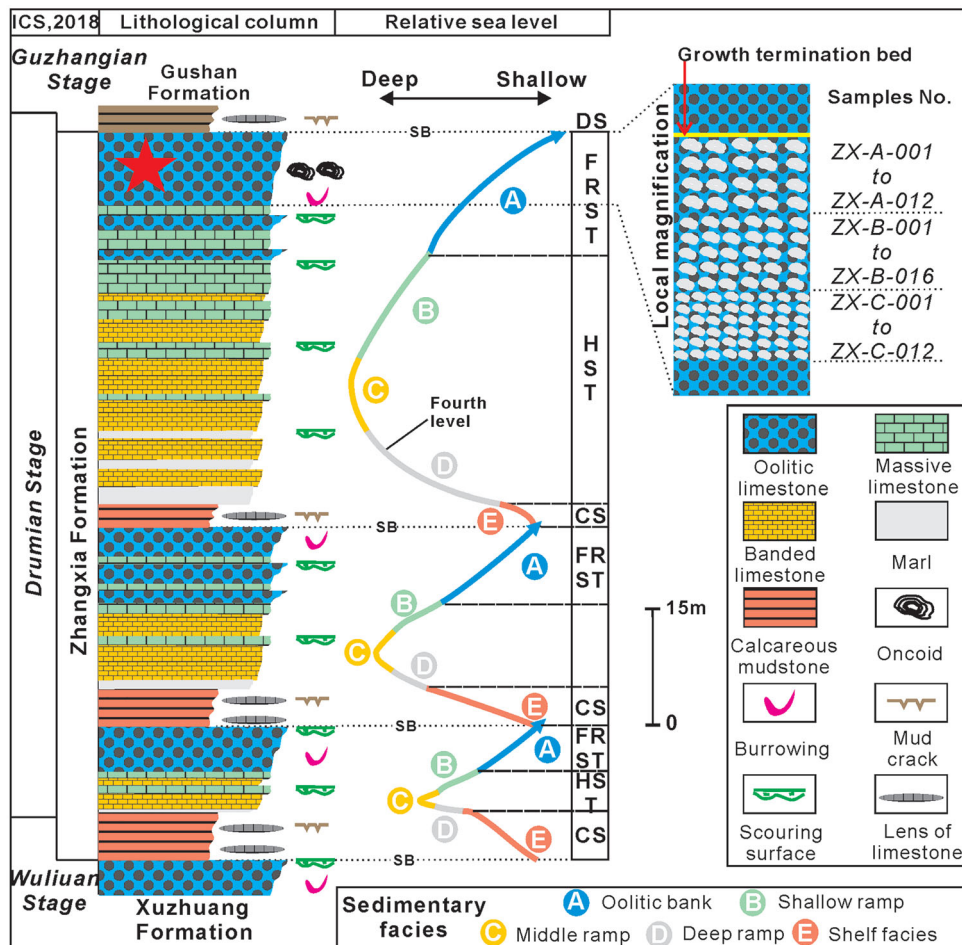


Figure 2. Sequence stratigraphic column of the Zhangxia Formation in the Sandaogou section. FRST, forced regression systems tract; CS, condensed section; SB, sequence boundary; grey-white oncolite symbols represent the change in oncolite size (red star indicates the location of the oncolite samples and ZX-A-001 etc. represent the samples number).

Xuzhuang formations and the boundary between the Zhangxia and overlying Gushan formations both correspond with a facies change from grain bank facies to shelf facies (Figures 2 and 3d). These boundaries imply platform inundation events attributed to rapid increases in sea-level (Xiao *et al.*, 2018; Xiao, Mei, *et al.*, 2020; Xiao, Wang, *et al.*, 2020; Xiao, Zafar, *et al.*, 2020). The oolitic grain banks developed in the upper part of each subsequence show coated grains formed in a high-energy shallow water environment (Figures 2 and 3b, c). During these episodes, the carbonate factory produced sediment that was deposited progressively, thus resulting in the development of thin-layered deep-water deposits (condensed section, CS) (Figure 2). Additionally, the high-stand systems tract (HST) directly overlies the deep-water sediments, which is the typical trend of a drowning unconformity (Latif *et al.*, 2018; Riaz, Latif, *et al.*, 2019; Riaz, Xiao, *et al.*, 2019; Schlager, 1999; Schlager & Warrlich, 2009; Xiao, Qin, *et al.*, 2017; Xiao, Sui, Qin, *et al.*, 2017).

The strata of the Zhangxia Formation can be subdivided into three fourth-order sequences based on internal lithology and the cyclicity of sedimentary facies changes; each of these depositional sequences represents a CS, HST and forced regression systems tract (FRST) (Figures 2 and 3). In

each fourth-order sequence, the calcareous mudstone of shelf facies in the lower part represents the CS (Figure 2), the banded mudstone interbedded with oolitic limestone in the middle part is a subtidal m-scale cycle and represents the HST, and the massive oolitic limestone in the upper part constitutes the FRST (Figure 2). Moreover, the top and bottom margins of each subsequence represent the distinctive sequence boundary of a drowning unconformity that developed owing to rapid sea-level rise (Latif *et al.*, 2018; Riaz, Latif, *et al.*, 2019; Riaz, Xiao, *et al.*, 2019; Schlager, 1999; Schlager & Warrlich, 2009; Xiao, Qin, *et al.*, 2017; Xiao, Sui, Qin, *et al.*, 2017).

Materials and methods

This study was based on field observations, measurements and laboratory tests on 40 oncolitic-oolitic limestone samples collected from the upper part of the third fourth-order sequence of the Cambrian Zhangxia Formation exposed in the Sandaogou section (Figure 2). Investigations were conducted at five scales, *i.e.* the mega- (\sim m), macro- (\sim dm), meso- (\sim cm), micro- (\sim mm to \sim μ m) and ultra-microscales

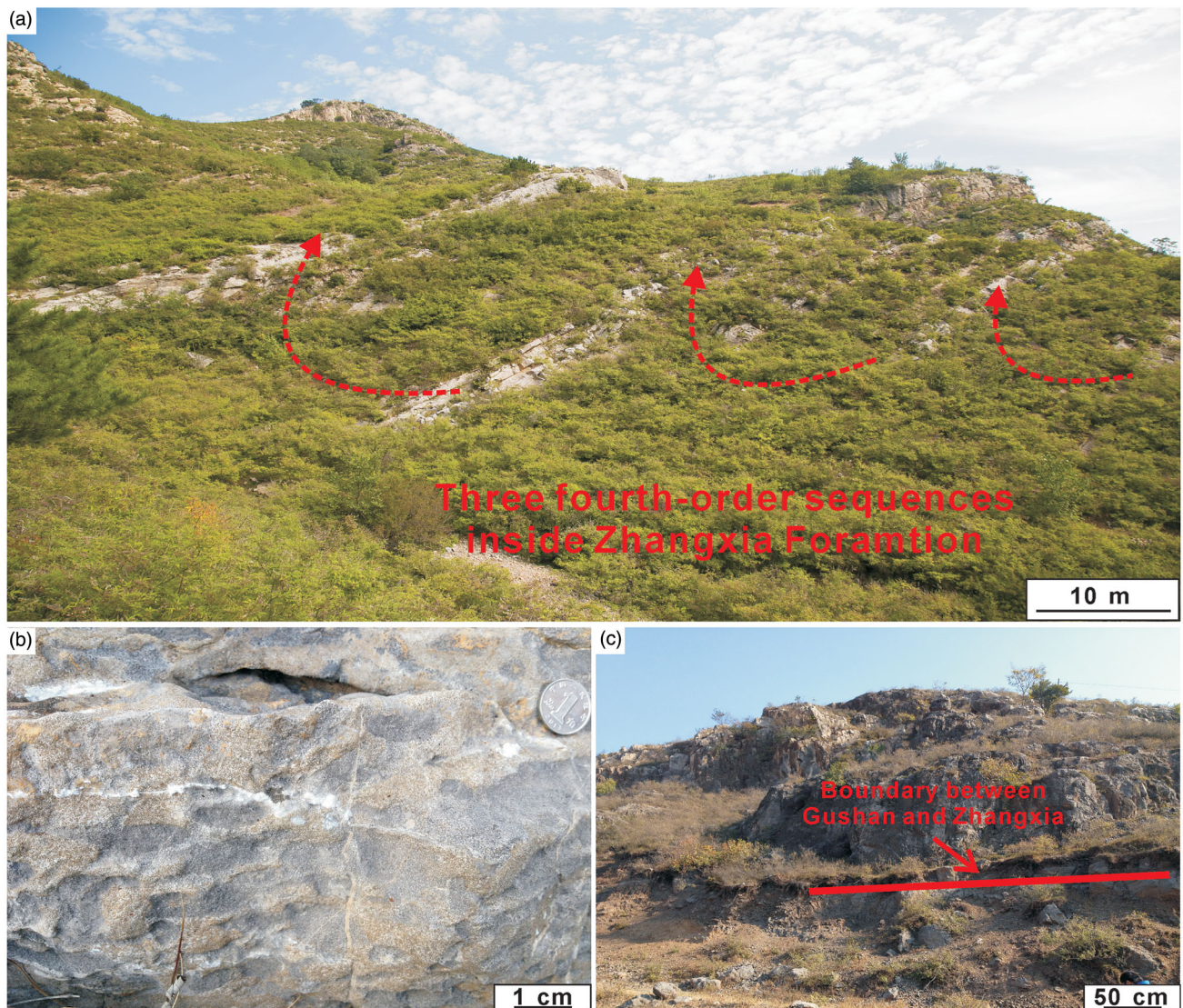


Figure 3. Sedimentary features of the Cambrian Miaolingian Series strata in the Sandaogou section. (a) Three fourth-order sequences in the Zhangxia Formation; (b) oolitic limestone in the middle part of the Zhangxia Formation; and (c) sequence boundary between the Zhangxia Formation and the Gushan Formation.

($\sim\mu\text{m}$ to $\sim\text{nm}$). The mega-macroscale study includes the compilation of the lithological column of the Cambrian (Miaolingian) Zhangxia Formation in the Sandaogou section (Figure 2) and the oncolite outcrops. The mesoscale research includes sampling the non-weathered and representative oncolites and measurement of their vertical size variation. Additionally, at the microscale microfacies analyses (cross-polarised light [XPL] and plane-polarised light [PPL]) were carried out on polished samples to observe the main lithological and biological components. Ultra-microscale observations, which rely on the SEM analyses of the nanofacies, were performed on polished thin-sections and freshly broken surfaces. Least altered samples from each section were broken into small pieces of $\sim 1\text{cm}^3$ and placed into FEI Quanta 200F scanning electron microscope for secondary electron imaging. The semiquantitative elemental analyses of submicron-sized spots were measured by

energy-dispersive X-ray spectroscopy (EDX) at 10.0 kV with current pulse between 11.24 and 49.21 kcps.

Carbon and oxygen isotope analyses were carried out on 15 micro-drilled oncolite samples dissolved in orthophosphoric acid. These samples were collected from areas without noticeable alteration, then sampled to avoid calcite veins and neomorphic processes. Isotope values were measured by a Thermo Scientific Delta V Advantage continuous flow isotope ratio mass spectrometer and are presented in delta (δ) notation relative to the Vienna Pee Dee Belemnite (VPDB) standard. The precision of $\delta^{13}\text{C}$ and $\delta^{18}\text{O}$ values for duplicate analyses was better than 0.1 ‰. Bulk mineral compositions were determined by XRD analyses on the prepared powder sample using the Bruker D2 PHASER instrument. All SEM and geochemical analyses of oncolite samples were performed in the State Key Laboratory of Oil and Gas Geology and Exploitation, Chengdu University of Technology.

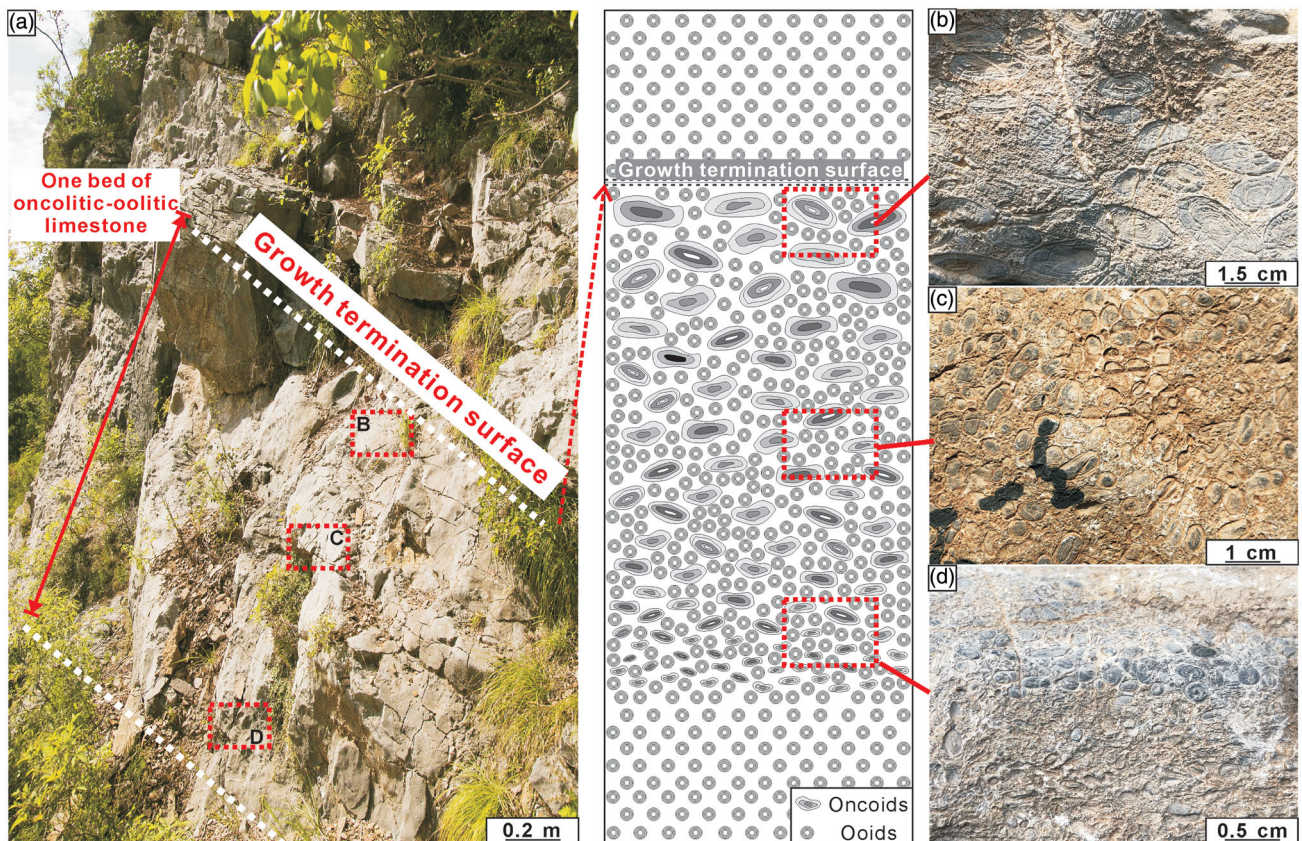


Figure 4. Macroscopic characteristics of oncooids in the Cambrian Miaolingian Series in the Sandaogou section. (a) Bed of oncolitic–oolitic limestone in the top part of the Zhangxia Formation (oolites in millimetres and oncooids in centimetres); (b) oncooids from the upper part of the thin bed, with large individual diameters of ~ 1.5 cm; (c) oncooids from the middle part of the thin bed, with moderate individual diameters of ~ 1 cm; and (d) oncooids from the lower part of the thin bed, with small individual diameters of ~ 0.5 cm.

Results

Macroscopic characteristics of oncooids

A widespread and exceptionally well-exposed bed of oncolitic–oolitic limestone (~ 4.5 m) occurs in the top part of the Zhangxia Formation in the Sandaogou section (Figures 2 and 4a). Macroscopically oncooids and ooids vary significantly in size (Figure 4b–d), and most of the oncooids have a nucleus, concentric laminae, observable cortex and a diameter of 0.2–2.4 cm.

The most striking phenomenon is that oncooids are small at the bottom of the bed and increase in size upward (Figure 4b–d). Moreover, our analyses of the Zhangxia Formation reveal that the oncooids disappear abruptly at the top of the massive oolitic limestone, which suggests a noticeable oncooid growth termination surface exists (Figures 2 and 4).

Microscopic characteristics of the oncolitic–oolitic limestone

The microscopic study of oncooid samples from the Sandaogou section reveals that most of the oncooids are well developed, have rounded to subrounded shapes and possess a smooth outer cortex (Figures 5 and 6). Moreover,

most oncooids have nuclei composed of ooids surrounding trilobite or echinoderm debris and well-defined light and dark laminae (Xiao, Mei, *et al.*, 2020). Based on the microscopic characteristics of oncooids, including the development of laminae and the location and number of nuclei, the oncooids can be divided into three types following the Cambrian oncooid classification scheme (Xiao, Mei, *et al.*, 2020): concentric laminar, lateral growth and multicore oncooids (Table 1). Additionally, a special kind of carbonate grain composed primarily of dark micrite is observed in the thin-section samples and reveals the diversity of carbonate grains in this Cambrian oolitic limestone.

Large numbers of filamentous *Girvanella* can be observed inside the oncooids. These filamentous microbial fossils are composed of a dark micrite sheath, with a main inner body composed of microspar (Riding, 2011; Xiao, Mei, *et al.*, 2020; Xiao, Zafar, *et al.*, 2020; Xiao *et al.*, 2018). These thin and elongated microorganisms are tubular, 0.7–2.5 mm in length and 15–60 μm in width, and subparallel to one another or tightly intertwined with each other (Figures 5 and 6). The external filament is characterised by thin-walled tubes made up of micrite, which is circular in the transverse section, and consist of calcite. These calcified microorganisms are generally regarded as the product of cyanobacteria calcification (Riding, 2011; Wang & Xiao,

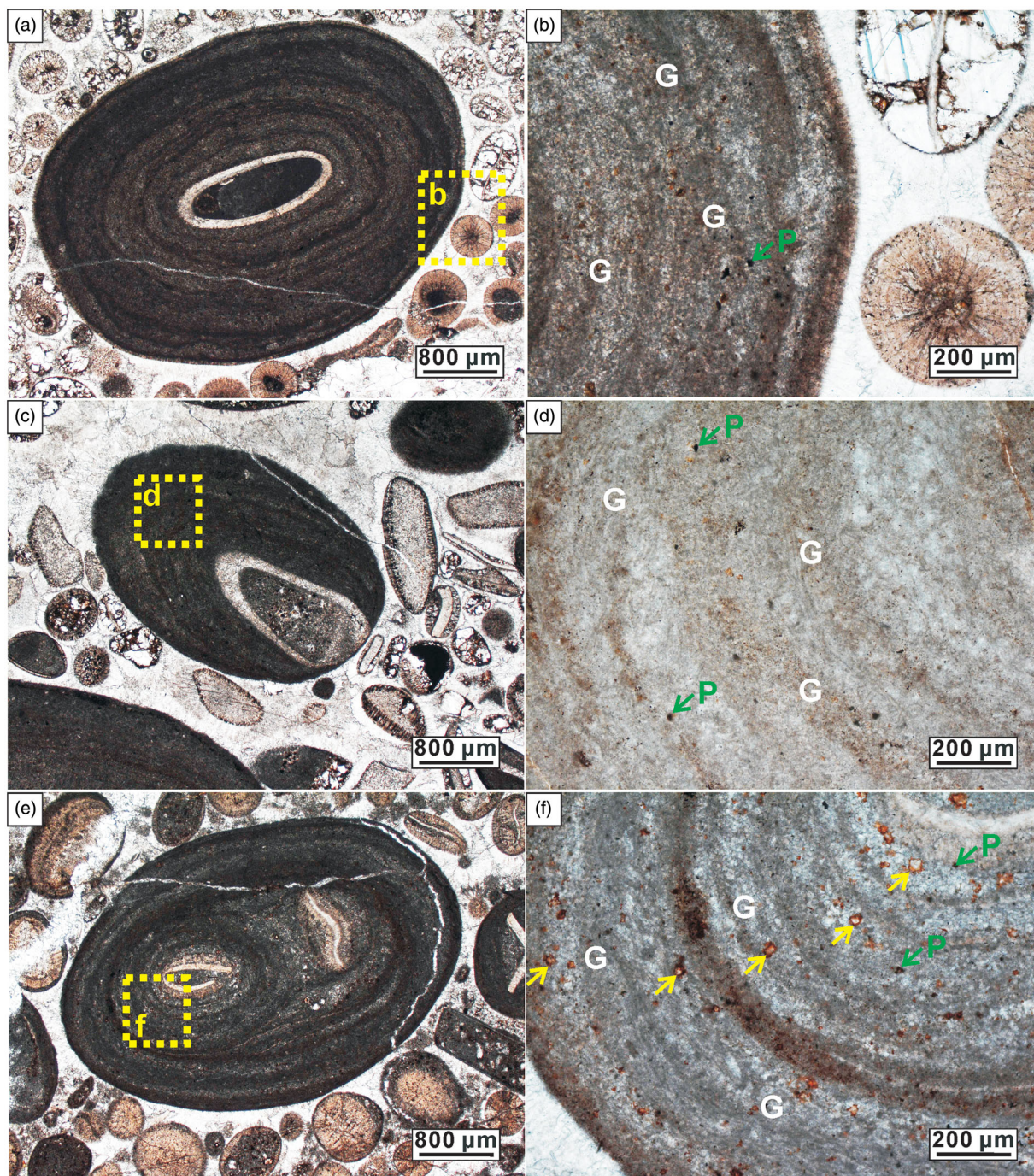


Figure 5. Morphological classification of the three types of oncoids in the Zhangxia Formation in the Sandaogou section. (a) Concentric laminar oncoids; (b) local magnification of (a), showing dark micrite concentric laminae growth, pyrite particles and filamentous *Girvanella*; (c) lateral growth oncoids with fine concentric laminae and easily identifiable trilobite debris in the nucleus; (d) local magnification of (c), indicating dark micrite concentric laminae growth, pyrite particles and filamentous *Girvanella*; (e) multicore oncoids with two trilobite debris nuclei; and (f) local magnification of (e), showing dark micrite concentric laminae growth, pyrite particles and filamentous *Girvanella*; yellow arrow show the dolomite crystal structure characteristics as bright edge of fog centre (Roberts *et al.*, 2013). G, *Girvanella*; P, pyrite.

2018; Xiao *et al.*, 2018; Xiao, Zafar, *et al.*, 2020; Xiao, Mei, *et al.*, 2020) and represent the fossil evidence of cyanobacteria calcification events in geological history records (Latif *et al.*, 2019; Pratt, 2001; Riding, 2006; Riding & Liang, 2005; Xiao *et al.*, 2018).

Type 1 concentric laminar oncoids

Concentric laminar oncoids represent the basic typical structure of oncoids (Figure 5a, b) (Védrine *et al.*, 2007). These oncoids have an average size of 0.6–1.4 cm and contain a nucleus, concentric light and dark laminae, and a

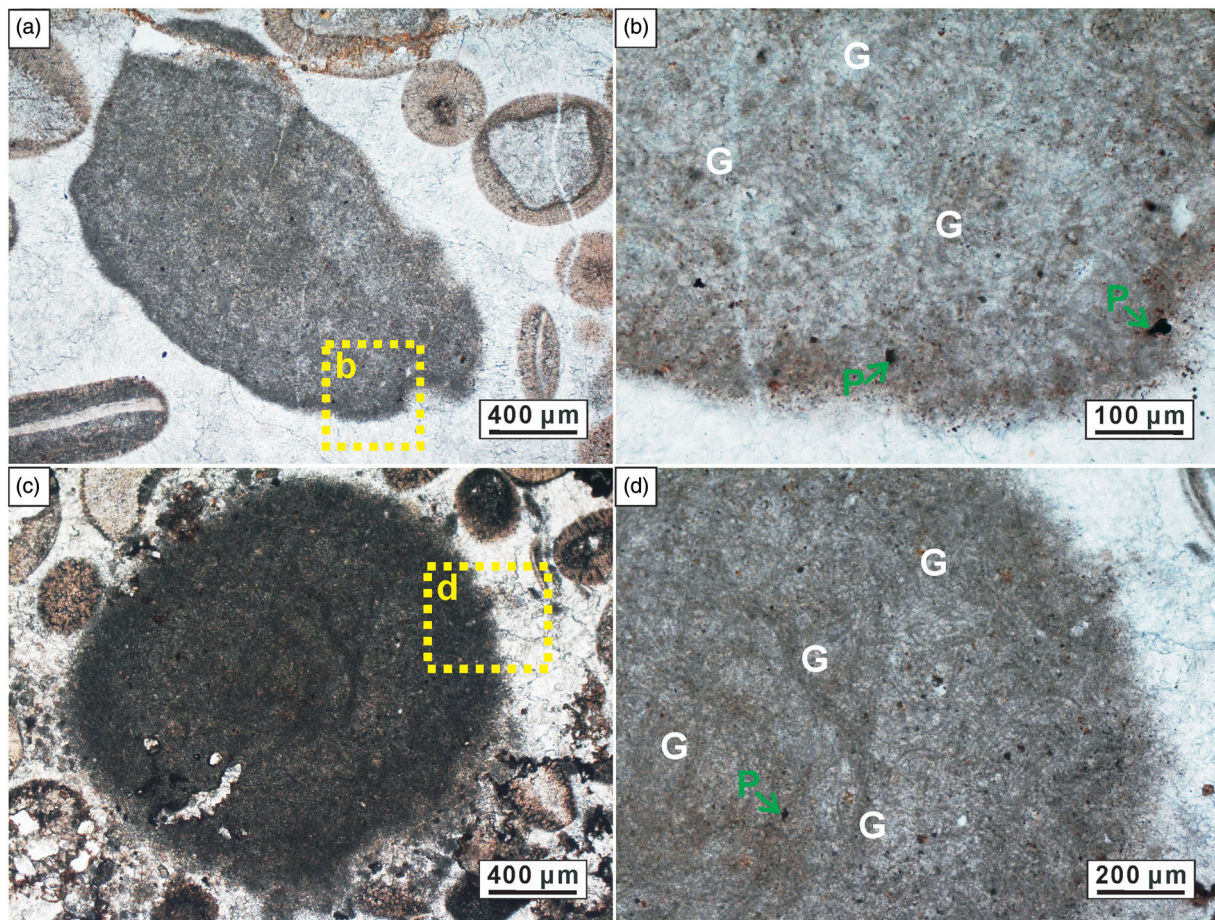


Figure 6. Microscopic characteristics of *Girvanella*-rich grains. (a) A *Girvanella*-rich grain with an irregular shape; (b) local magnification of (a), indicating the disordered and intertwined *Girvanella* fossils; (c) a *Girvanella*-rich grain with a regular shape and a diffuse edge; and (d) local magnification of (c), indicating the disordered and intertwined *Girvanella* fossils. G, *Girvanella*; P, pyrite.

Table 1. Mineral composition content of oncolitic limestone from Zhangxia Formation in Sandaogou section.

Sample no.	Mineral composition content (%)					
	Quartz	K-feldspar	Calcite	Dolomite	Pyrite	Clay mineral
ZX-A-001	1		94	5		
ZX-A-002	1	1	95	3		
ZX-A-003	2		95	2		1
ZX-A-004	2	1	94	2	1	
ZX-A-005	1		94	4		
ZX-B-001	2	1	95	1		1
ZX-B-002	2		97		1	
ZX-B-003	2		95	2		1
ZX-B-004	2	2	94	1	1	
ZX-B-005	1		96	1		2
ZX-C-001	1		96	1	1	1
ZX-C-002	1		95	2		2
ZX-C-003	2		96			1
ZX-C-004		1	98		1	
ZX-C-005	1		98	1		2

smooth cortex, similar to widely reported oncolid morphological characteristics (Li *et al.*, 2000; Reolid & Nieto, 2010; Schaefer *et al.*, 2001; Shi & Chen, 2006; Wang & Xiao, 2018; Xiao, Latif, *et al.*, 2018; Xiao, Zafar, *et al.*, 2020; Yang *et al.*, 2011). The shape of the Type 1 oncolid is regular and generally circular or elliptical, and the laminae are generally 50 µm thick (Figure 5a). Filamentous microbial fossils are

visible inside the laminae with characteristics that are consistent with the classical identification of *Girvanella* (Xiao *et al.*, 2018).

Type 2 lateral growth oncolids

The main features of lateral growth oncolids (Figure 5c, d) include alternating light and dark laminae (Wang & Xiao, 2018; Xiao, Mei, *et al.*, 2020; Xiao, Zafar, *et al.*, 2020), symmetrical shapes, average size (0.8–2.2 cm) and a nucleus composition (trilobite debris) similar to that of the Type 1 oncolid. The noticeable difference between Type 1 and Type 2 oncolids is that the nucleus of the Type 2 oncolid is not present at the centre of the oncolids (Figure 5c). On one side of the nucleus, the laminae are thicker and well developed, whereas on the other side, the laminae are thinner and poorly developed (Figure 5c). In addition, rare dispersed calcite microcrystals are present inside the laminae and mostly appear on the side with better developed laminae. The occurrence of these calcite grains does not appear to have produced a severe negative impact on the development of laminae and may be interpreted as bubbles, produced as a by-product of photosynthetic organisms that were later infilled by calcite

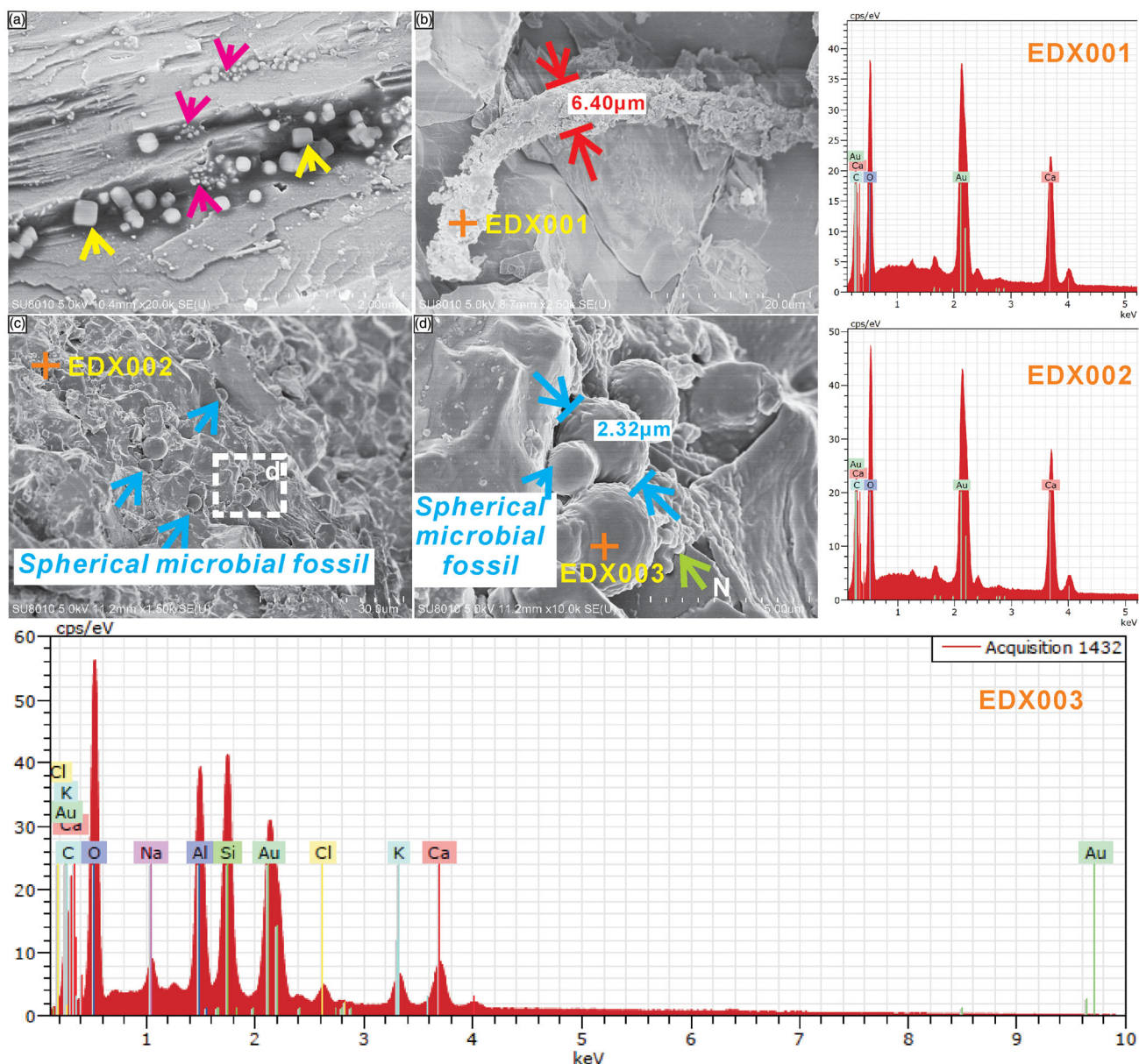


Figure 7. Ultra-microscale fabric of micrite within oncoids in the Zhangxia Formation in the Sandaogou section and the EDX results. (a) Two types of pyrite grains occur inside the micrite: pink arrows indicate framboidal pyrite grains and yellow arrows indicate normal pyrite grains; (b) filamentous microbial fossils inside the dark micrite; (c) spherical calcified microorganism fossils (blue arrows) inside the dark micrite; and (d) local magnification of (c), showing nanospheres (green arrow) growing around spherical calcified microorganism fossils.

(Wilmeth *et al.*, 2015). Pyrite grains are also present inside the laminae of the oncoids (Figure 5d).

Type 3 multicore oncoids

Multicore oncoids (Figure 5e, f) typically have a distinctive shape and contain at least two nuclei (Figure 5e). The inner laminae near each nucleus are commonly concentric, whereas outer laminae are composed of a large number of light microspar and dark micrite laminae surrounding multiple nuclei to form a single multicore oncoid. The multicore oncoids are irregular in overall shape with average sizes ranging from 0.9 to 2.3 cm. Some oncoids exhibit round or subrounded shapes, and their nuclei are mostly

composed of trilobite debris or ooids. More importantly, the *Girvanella* fossils present in multicore oncoids feature winding and amorphous patterns (Figure 5f). The multicore oncoids contain fine-scale light and dark laminae, analogous to Type 1 oncoids (Figure 5a).

Girvanella-rich grain

In addition to the oncoids, a special kind of grain is observed inside the oncolitic–oolitic limestone (Figure 6a–d). At a microscopic scale, these grains feature a rounded to subrounded shape, with no obvious nucleus or laminae structure, and a composition dominated by dark micrite (Figure 6a–d). Important features that distinguish

these grains from the oncoids are the rough edges with no obvious cortical wrapping (Figure 6a). Notably, the average size (0.2–0.6 cm) of these grains is smaller than that of the three types of oncoids discussed. Compared with the abundance of *Girvanella* in oncoid types 1, 2 and 3, filamentous *Girvanella* fossils are abundant in the interiors (Figure 6b, d) and feature winding and amorphous characteristics. Numerous pyrite grains are present inside the grains (Figure 6b, d). We refer to these grains as *Girvanella*-rich grains.

Ultra-microscopic characteristics of oncoids

SEM and EDX techniques were employed for precise observation of ultra-microscopic oncoid characteristics and for qualitative elemental analysis. The results indicate that there are two types of pyrite grains with dark micrite, massive pyrite and framboidal pyrite grains (Figure 7a). The occurrence of framboidal pyrite grains supports the microbial origin of the oncoid varieties because framboidal pyrite is associated with sulfate-reducing bacteria (SRB), and microbial metabolism stimulates carbonate precipitation

Table 2. Carbon and oxygen isotope values of oncolitic limestone samples from the Zhangxia Formation in the Sandaogou section.

Sample no.	$\delta^{13}\text{C}$ (‰ VPDB)	$\delta^{18}\text{O}$ (‰ VPDB)
ZX-A-001	-0.46	-9.62
ZX-A-002	-0.57	-7.69
ZX-A-003	-0.52	-8.71
ZX-A-004	-0.66	-9.11
ZX-A-005	-0.56	-8.48
ZX-B-001	-0.73	-9.01
ZX-B-002	-0.79	-7.22
ZX-B-003	-0.77	-8.39
ZX-B-004	-0.88	-9.59
ZX-B-005	-0.93	-9.27
ZX-C-001	-1.08	-9.77
ZX-C-002	-0.91	-8.62
ZX-C-003	-0.93	-8.29
ZX-C-004	-1.03	-9.14
ZX-C-005	-1.11	-8.59

(Baumgartner *et al.*, 2006; Xiao, Sui, Latif, *et al.*, 2017; Xiao, Wang, *et al.*, 2020).

Mineral compositions are shown in the EDX results. The dark micrite is composed of calcium carbonate mud with a low degree of crystallisation (Figure 7c). Most notably, the dark micrite inside oncoids contains two kinds of microbial fossils, spherical and filamentous microbial fossils, which are surrounded by nanospheres (Figure 7b, d). The EDX results indicate that the oncoids and the main body of the filamentous microbial fossils are composed of CaCO_3 (EDX001). However, the elemental composition of the spherical microbial fossils (EDX003) includes Al, Si, K, Na and Cl, indicating distinct compositional differences between the spherical and filamentous fossils. The data and elemental mapping indicate that the main body of the spherical microbial fossils may be composed of calcium carbonate and clay minerals (Diaz *et al.*, 2017; Fariás *et al.*, 2014; Zhu *et al.*, 2018).

Mineralogical and isotope results

An XRD analysis was performed to evaluate the mineral compositions of 15 oncolitic–oolitic limestone samples from the upper part of the Zhangxia Formation (Table 2). The oncolitic limestone is primarily composed of calcite. The crystal structure (Figure 5f) shows that dolomites are secondary (Roberts *et al.*, 2013) and may represent the products of the depositional environments shallowing process during relative sea-level fall (Figure 2) (Guo *et al.*, 2020; Liu & Zhang, 2012, 2015; Xiao, Mei *et al.*, 2020; Xiao, Sui, Latif *et al.*, 2017). The presence of quartz and feldspar (Table 1) implies input of terrigenous materials during the limestone deposition with the interaction between land and offshore shallow water.

The carbon and oxygen isotope values (Table 2) have narrow ranges with $\delta^{13}\text{C}$ values between -1.11 and -0.46 ‰ VPDB and $\delta^{18}\text{O}$ values between -9.77 and

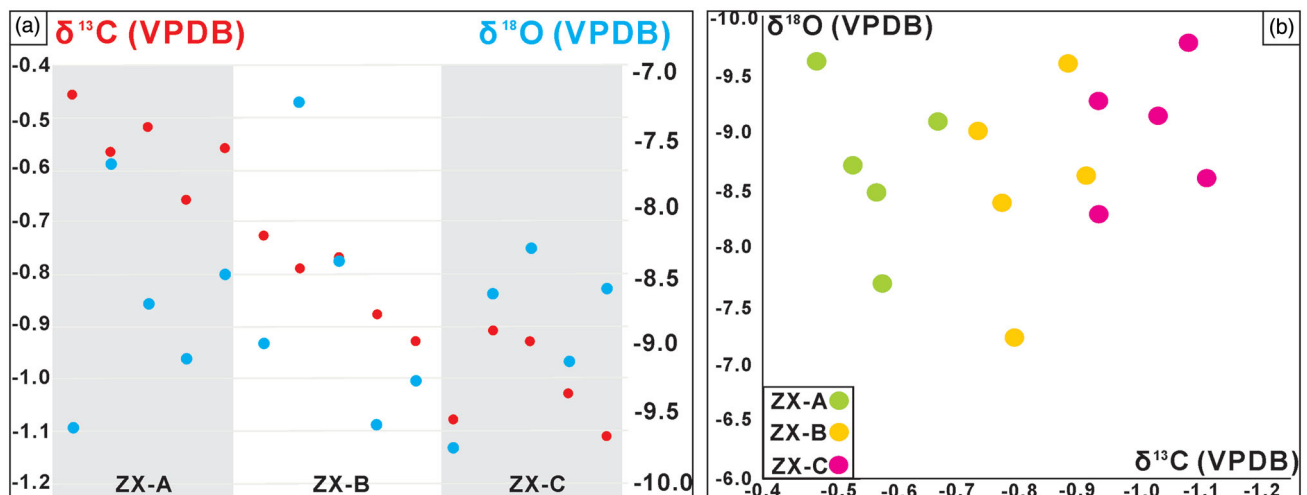


Figure 8. (a) Plot of $\delta^{13}\text{C}$ (VPDB) and $\delta^{18}\text{O}$ (VPDB) values with depth show that the isotopic characteristics of the three groups of oncoids samples. It can be seen that $\delta^{18}\text{O}$ has no obvious regularity. However, $\delta^{13}\text{C}$ of ZX-A shows the higher value and lower in ZX-C. (b) Scatter plot of $\delta^{18}\text{O}$ values vs $\delta^{13}\text{C}$ for the oncolitic limestone from the Cambrian Zhangxia Formation (Miaolingian Series) in the Sandaogou section.

–7.22‰ VPDB (Figure 8). The $\delta^{18}\text{O}$ values show no obvious trends, but $\delta^{13}\text{C}$ values become more positive upward in the section (Table 2).

Discussion

Previous studies have reported that the genesis of marine carbonate oncoids is predominantly related to microorganisms (Han *et al.*, 2015; Wang & Xiao, 2018) but much of the evidence of microbial is based on oncoids that have been affected by diagenesis and incompletely preserved (Dupraz *et al.*, 2009). Some well-preserved evidence of microorganisms related to the formation of oncoid laminae can be observed at microscopic and ultra-microscopic scales (Qi *et al.*, 2016; Wang & Xiao, 2018) with morphology reflecting the marine environment during oncoid formation (Védrine, 2008; Védrine *et al.*, 2007) and have been considered as evidence of paleo-environmental events preserved in the geological record (such as anoxic events) (Zhang *et al.*, 2014). Therefore, microscopic and ultra-microscopic morphology of oncoids can have fundamental implications for the study of paleogeography and paleoenvironments (Dahanayake, 1977; Flügel & Munnecke, 2010; Gradziński *et al.*, 2004; Jones, 1992; Jones & Renaut, 1997, 2010; Peryt, 1983; Yang *et al.*, 2011; Zhang *et al.*, 2015).

Origin of oncoids and *Girvanella*-rich grains

Research and classification methods on oncoids have focussed on three aspects: (1) morphological classification (Dahanayake, 1977; Han *et al.*, 2015; Peryt, 1983); (2) mineral component classification (Flügel & Munnecke, 2010); and (3) forming environment classification (Védrine *et al.*, 2007; Yang *et al.*, 2011).

Based on the microscopic observations of the oncoids (Figures 5 and 6), the arrangement of *Girvanella* in these carbonate grains from the Zhangxia Formation can be summarised as follow. (1) In the oncoids with clear alternations between light and dark laminae, a small number of *Girvanella* filaments in the dark laminae are oriented parallel to the boundary between light and dark laminae, whereas the *Girvanella* filaments in the light layer are oriented perpendicular to the boundary. This growth pattern mainly occurs in oncoids that have obvious alternating light and dark laminae, larger size and regular shapes (Figure 9a). (2) In other oncoids (Figure 9b), the arrangement of the *Girvanella* filaments is perpendicular to the boundary between the light and dark laminae, but in these oncoids, the arrangement is controlled not by the *Girvanella* but by the type of support (micrite or microspar) around the filaments (Figure 9b). This *Girvanella* growth pattern mainly occurs in oncoids that have alternating light and dark laminae with diffuse boundaries and tend to be irregular in shape and medium in size. (3) In a third growth pattern distinct from the first two types (Figure 9c), the *Girvanella* filaments are intertwined and linked with each

other without any obvious directionality, showing a relatively disordered growth state. This growth mode mainly appears in oncoids with no obvious light and dark laminae (Figure 9c) and is observed only in *Girvanella*-rich grains.

Studies on modern microbialites have shown that the arrangement of filaments reflects the formation process during the construction of stromatolites by cyanobacteria-dominated microbial mats (Bosak *et al.*, 2009; Jones *et al.*, 2005). In this study, the arrangement of the filaments demonstrates that differences exist among these formation processes. Oncoids with obvious directional arrangement of *Girvanella* in dark laminae and those with a vertical arrangement of filaments suggest different responses of microbial mats to light factors in different depositional environments (water depth). The disordered and intertwined filaments appeared in the smaller grains dominated by dark micrite that are more common in the lower part of the oncoid bed and reflect the disorder of filamentous microorganisms in cyanobacterial mats in deeper-water environments. A large number of microbial fossils, including spherical and filamentous microbial fossils (Figure 9), and microbial-related precipitates (nanospheres and framboidal pyrite) (Figure 9a, d) are observed in the oncoid structures. These features, which are clearly associated with microorganisms, imply that the origin of these oncoids is linked to the calcification of cyanobacteria-dominated microbial mats (composed of *Girvanella* filaments) and the degradation of heterotrophic bacteria-produced framboidal pyrite particles (Xiao, Sui, Latif *et al.*, 2017; Xiao, Mei *et al.*, 2020) (Table 3).

Size variation and distribution of oncoids

Studies have shown that the morphological characteristics of oncoids to some extent reflect changes in the dynamic conditions of the seawater (Védrine, 2008; Védrine *et al.*, 2007). In the present study, the most remarkable trend is that the size of the oncoids in the Zhangxia Formation progressively increases from bottom to top of the bed (Figures 2 and 4). The average size of the individual oncoids at the bottom is relatively small (~0.5 cm) contrasting with the average size of the oncoids of ~1.0 cm from the middle part of the oncoid bed and an average size of 1.5 cm at the top (Figures 4 and 10). The Type 1 oncoids are distributed throughout the bed of oncolitic limestone, but their proportion and size increase upward; types 2 and 3 oncoids are abundant in the middle and upper parts of the oncoid bed. The *Girvanella*-rich grains mainly occur in the bottom part of the oncoid bed and are smallest in size and lowest in proportion in the middle and upper parts of oncoid bed (Figure 10).

The macroscopic study of oncoids outcrops has shown that the top part of the Zhangxia Formation, where the oncoids bed is located, can be confirmed by the upward-shallowing trend (Figure 2). Mineral composition result shows that the mean content of dolomite in oncoid

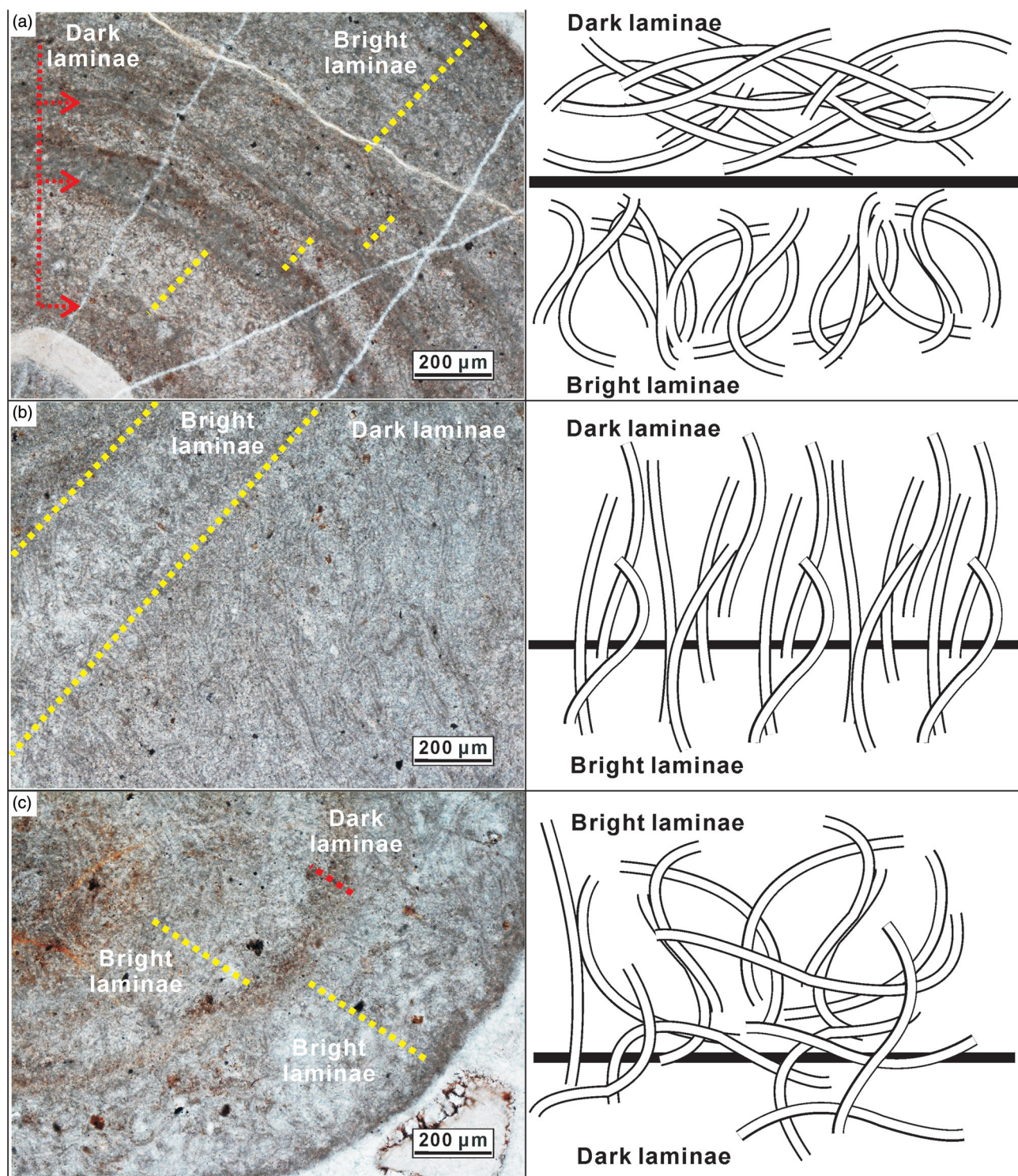






Figure 9. Examples of the three different arrangements of *Givvanella* fossils inside oncoids. (a) Most common arrangement of *Givvanella* fossils inside oncoids. The filaments in the dark laminae are parallel to the interface, whereas the filaments in the light laminae are perpendicular to the interface. This arrangement mainly occurs inside large oncoids with clear micritic and microspar laminations; (b) the filaments of *Givvanella* are perpendicular to the boundary of light and dark laminae; and (c) disordered and intertwined arrangement of *Givvanella* fossils. This arrangement mainly occurs inside *Givvanella*-rich grains and small oncoids composed of homogeneous micrite.

samples with larger oncoids is higher than that of the samples with smaller oncoids (Table 1; Figures 8 and 11). Microscopic research shows that the dolomite crystal inside the oncoids should be interpreted as the dolomitisation

products owing to depositional environmental shallowing progress (Guo *et al.*, 2020; Liu & Zhang, 2012, 2015; Xiao, Mei *et al.*, 2020; Xiao, Sui, Latif *et al.*, 2017). This is in line with the macroscopic sedimentological interpretation of

Table 3. Classification and origin summary of oncooids from Cambrian Miaolingian Series.

Type of oncooids	Given name in this research	Diameter of oncooids	Microbial fossil and pyrite	Origin summary
Type 1 	Concentric laminar oncooids	0.6–1.4 cm	<i>Girvanella</i> , pyrite	Spherical stromatolites (Krumbein & Cohen, 1977). Envelope growth of algae adhering to granules (Zeng <i>et al.</i> , 1983). Degradation of heterotrophic bacteria and algae residues in microbial mats (Mesozoic reports related to diatoms) (Gerdes <i>et al.</i> , 1994). Cyanobacteria calcification and EPS degradation cooperate strong hydrodynamic force (Wang & Xiao, 2018; Xiao, Mei, <i>et al.</i> , 2020; Xiao, Wang, <i>et al.</i> , 2020).
Type 2 	Lateral growth oncooids	0.8–2.2 cm	<i>Girvanella</i> , pyrite	Cyanobacteria calcification and EPS degradation focusing on weight nucleus cooperate weak hydrodynamic force (Wang & Xiao, 2018; Xiao, Mei, <i>et al.</i> , 2020; Xiao, Wang, <i>et al.</i> , 2020).
Type 3 	Multicore oncooids	0.9–2.3 cm	<i>Girvanella</i> , pyrite	Bonding of microbial community on the surface of oncooids (Flügel & Munnecke, 2010). Encapsulation of biofilm (Wang & Xiao, 2018; Xiao, Mei, <i>et al.</i> , 2020; Xiaol, Wang <i>et al.</i> , 2020).
	<i>Girvanella</i> -rich grain 	0.2–0.6 cm	<i>Girvanella</i> , pyrite	Reworked microbialites intraclasts and clacimicrobe fragments (Han <i>et al.</i> , 2015). Calcified microbial mat remnants encapsulated by spherical biofilm (Wang & Xiao, 2018; Xiao, Mei, <i>et al.</i> , 2020; Xiao, Wang, <i>et al.</i> , 2020)

outcrops and reveals that the fall in relative sea-level resulted in a decrease in the accommodation space and an increase in the proportion of dolomitisation (Guo *et al.*, 2020; Liu & Zhang, 2012, 2015; Xiao, Mei *et al.*, 2020; Xiao, Sui, Latif *et al.*, 2017) (Figures 2 and 11).

The upward-shallowing depositional environment changes coupled with the change in oncooids size is also reflected in the geochemical analyses. The $\delta^{13}\text{C}$ values (Table 1; Figure 11) are more enriched in ^{13}C in the upper portion with larger average sizes of oncooids and more depleted in ^{13}C at the bottom with smaller average sizes of oncooids. Carbon isotope values of marine carbonate rocks can be affected by many factors, such as the ocean oxidation–reduction environment, the time of biological prosperity or extinction, volcanic activity, the generation or release of natural gas hydrate, the increase in organic carbon burial amount or burial rate, sea-level changes, structural activity and other geological conditions (Hoffman *et al.*, 1998; Horacek *et al.*, 2007; Kaufman & Knoll, 1995; Vinogradov, 2008; Xiao, Mei *et al.*, 2020; Xiao, Wang *et al.*, 2020). Previous studies have shown that the carbon isotope evolution in Cambrian carbonates is closely related to sea-level fluctuation and biodiversity evolution (Hoffman *et al.*, 1998; Kimura & Watanabe, 2001; Kouchinsky *et al.*, 2008; Zhu *et al.*, 2004). Evidence of increased diversity in archaeocyaths from the Siberia Cambrian strata (Brasier *et al.*, 1994) and reports of metazoan abundance increase from the Cambrian in South China (Ishikawa *et al.*, 2014) indicate

strong relevance with $\delta^{13}\text{C}$ change. These phenomena are interpreted as biological prosperity and photosynthesis improving the paleo-marine productivity (Peters & Gaines, 2012). The prosperity of organisms means that more ^{12}C is consumed in metabolism, which makes ^{13}C relatively enriched in sediments and recorded by positive carbon isotope drift events (Kaufman & Knoll, 1995; Kump & Arthur, 1999; Montaez *et al.*, 2000). In this study, $\delta^{13}\text{C}$ values coupled with oncooid sizes can be interpreted as: a shallowing environment that allows an increase in the activity of cyanobacteria-dominated microbial mats (Riding, 2012; Xiao, Zafar *et al.*, 2020; Xiao *et al.*, 2018); metabolism of microbial mats increases and is dominated by cyanobacteria (the builder of oncooids); and greater carbon sequestration leads to enriched $\delta^{13}\text{C}$ values (Xiao, Mei *et al.*, 2020; Xiao, Wang, *et al.*, 2020) an increase in the abundance of oncooids and an increase in size of individual oncooids at the top of the bed. In the deeper depositional environments, a reduction in carbon sequestration results in depletion of ^{13}C (Chen *et al.*, 2008; Vinogradov, 2008; Xiao, Wang, *et al.*, 2020).

Interpretation of growth termination surface and response to sea-level change

Growth termination surfaces at the top of the oncooid bed (Figures 2, 4a and 11) are comparable with surfaces reported for stromatolites (Bosak *et al.*, 2009, 2010; Mei &

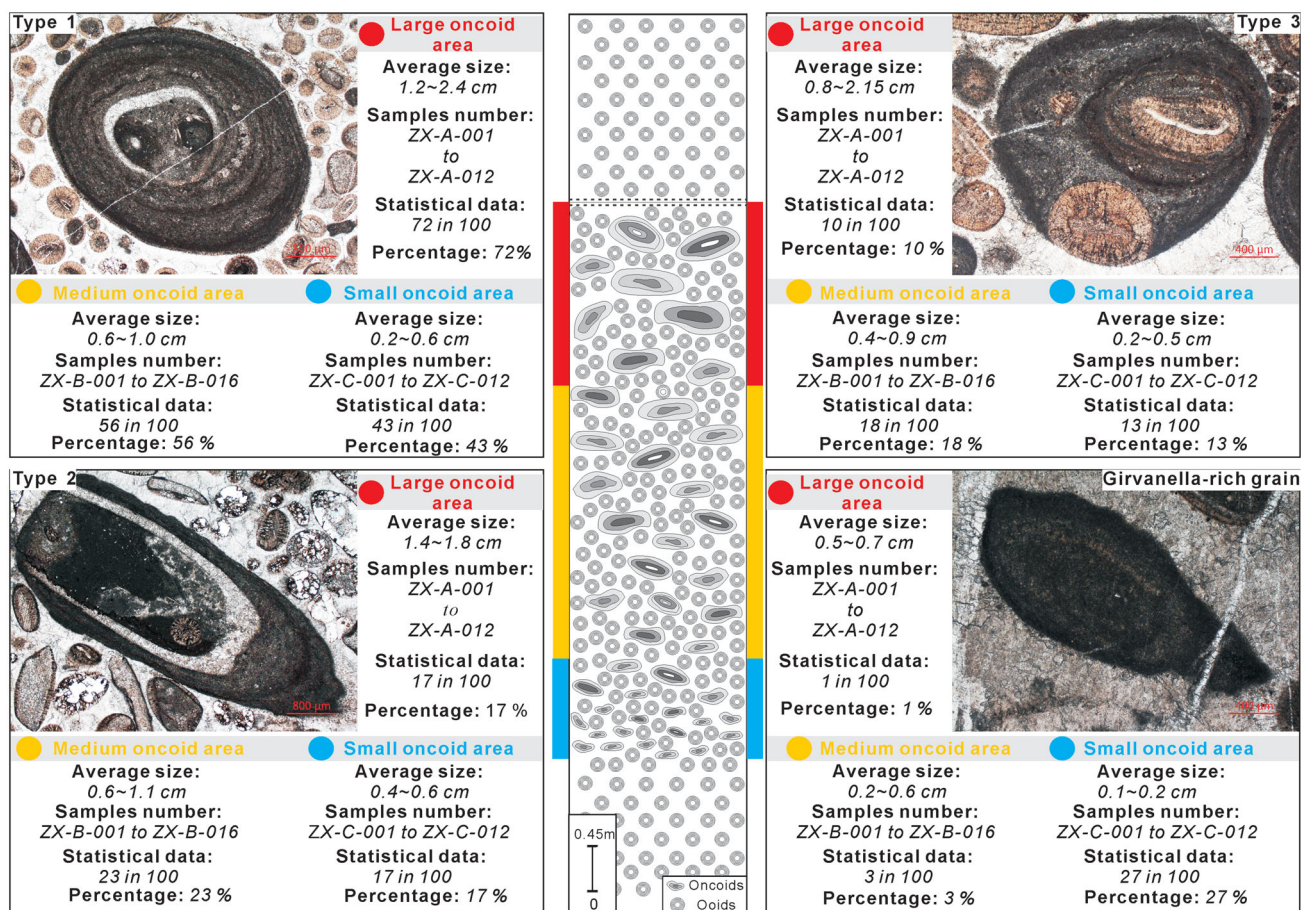


Figure 10. Size variations and distributions of the three types of oncoids and the *Girvanella*-rich grains. The data in this study come from the microscopic observation of samples from three regions. In the regions with large oncoids, medium-sized oncoids and small oncoids, we randomly selected 100 carbonate particles larger than ooids. According to the morphological classification in this paper, the percentages of the four particle types were calculated.

Gao, 2015) and suggest that changes in depositional environments affect the photosynthetic microbial mats. The appearance of the termination surface also represents the cessation of microbial activity.

Our findings demonstrate that the size of individual oncoids gradually increases from the bottom to the top of the bed (Figures 2, 4b–d and 11) and that oncoids near the growth-termination surface are well developed in terms of size (maximum individual sizes) and micromorphology (clear nuclei, alternating laminae and clear boundaries for light laminae) (Figures 5–7). Therefore, the benthic cyanobacterial microbial mats reached a maximum stage of development just before the formation of the growth-termination surface. The sequence stratigraphic framework (Figure 2), combined with the carbon and oxygen isotope values (Figure 11), shows that the oncolitic–oolitic limestone bed at the top of the Zhangxia Formation formed in a FRST. In this systems tract, seaward movement of shoreline in response to sea-level fall (Latif *et al.*, 2018; Riaz, Latif *et al.*, 2019; Xiao, Qin, *et al.*, 2017; Xiao, Sui, Qin, *et al.*, 2017), led to decreases in the sediment accommodation space and relative sea-level and shallowing of the depositional environment. This relative sea-level change was already confirmed in $\delta^{13}\text{C}$ values, consistent with

mineralogy and macrocosm (Figure 11), with oncoids more extensively developed in shallow environments and more restricted in deeper environments.

The sedimentary processes in the Zhangxia Formation can be divided into four stages (Figure 12). (1) A third fourth-order sequence is associated with the late high-stand system deposits beginning at the end of early high-stand deposits and led to the formation of oolitic limestone (Figure 2). Owing to the relatively deep-marine environment and large amount of sediment input into the accommodation space, the light energy available to benthic microbial mats dominated by cyanobacteria (*Girvanella*) was relatively limited and unsuitable for the unstable microbial mats to produce oncoids (Figure 12a). (2) With the decrease in relative sea-level, the sedimentary accommodation space progressively decreased, and the shallowing of the water resulted in an increase in the light available to benthic cyanobacterial microbial mats leading to their gradual growth during this period. During this stage, smaller oncoids were produced inside the microbial mat (Figure 12b). (3) With a further decrease in relative sea-level and accommodation space, the depositional environment gradually reached the most suitable environment for benthic cyanobacteria microbial mat development.

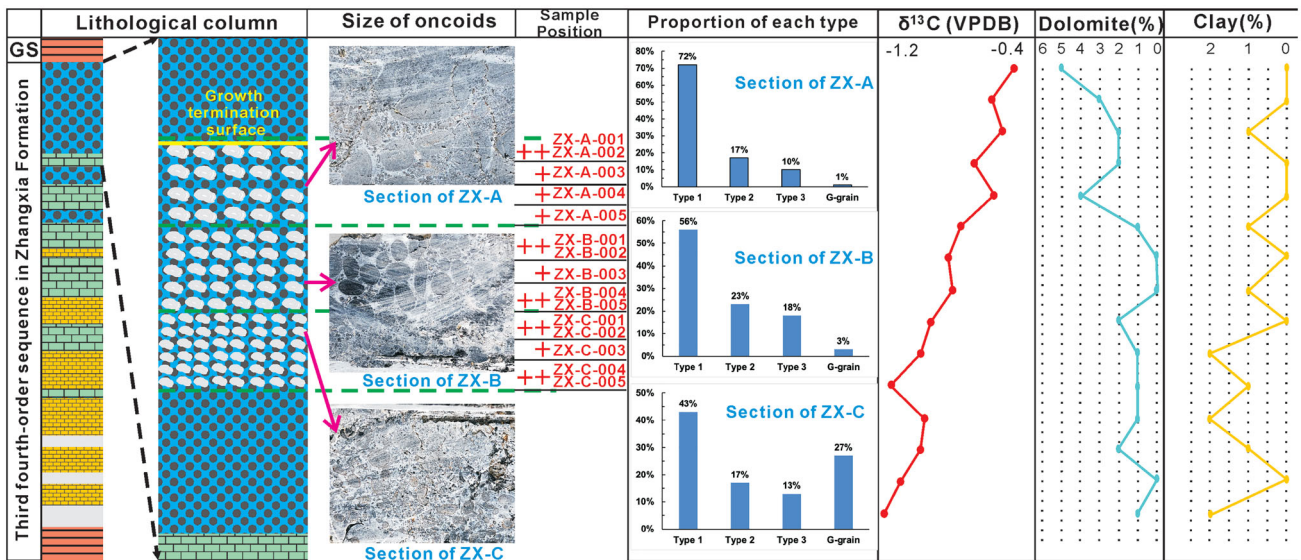


Figure 11. Integration of the stratigraphy, oncoïd size, sampling points, geochemistry and occurrence of different types of oncoïds in the Zhangxia Formation in the Sandaogou section. Dolomite and clay minerals composition data from the XRD results.

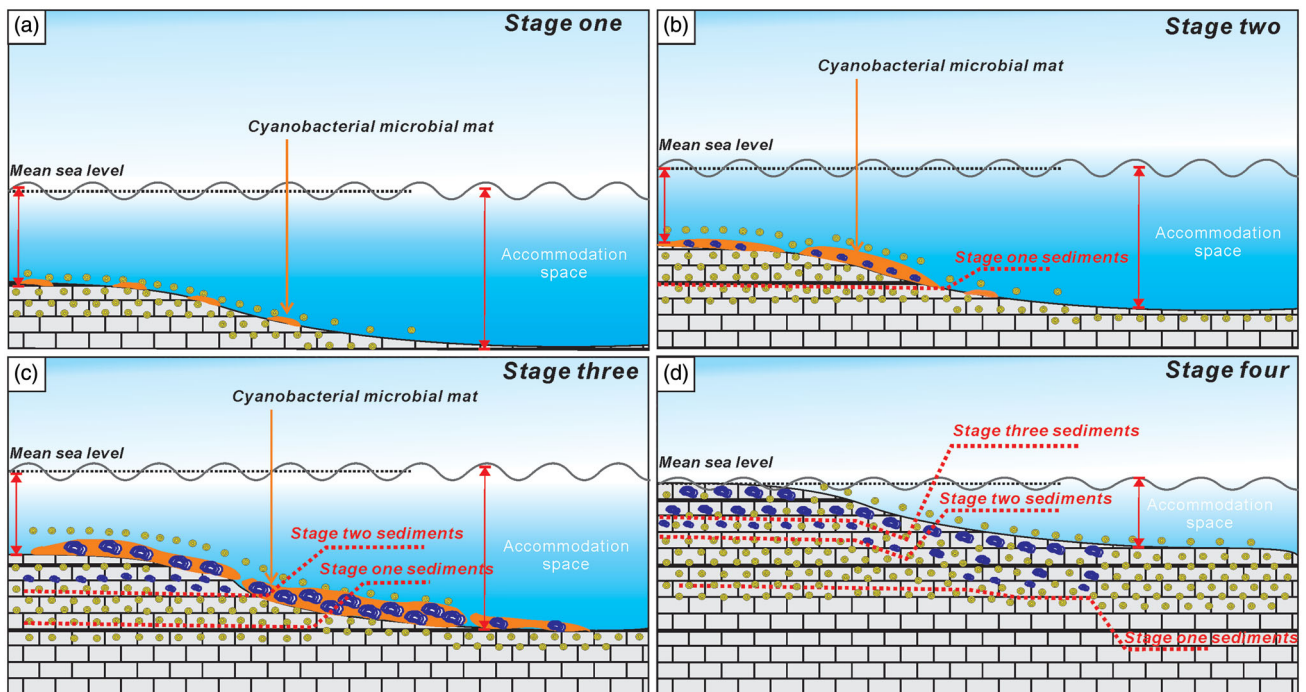


Figure 12. Depositional process of oncolitic–oolitic limestone during the forced regression and the evolution of the oncoïds associated with the cyanobacterial microbial mat. (a) End stage of HST in the top fourth-order sequence in Figure 2. Owing to the previous transgression, the depositional environment was deeper. The low light intensity of benthic cyanobacteria microbial mat reception with poor growth conditions for cyanobacteria with no oncoïds formed in this stage. (b) With the gradual decrease in relative sea-level, the depositional environment in the second stage became shallower, and the light intensity reception of benthic cyanobacterial microbial mat increased. Microbial mats began to flourish, and small oncoïds were formed. (c) With shallowing of water body, the light intensity reception of benthic cyanobacteria microbial mats gradually increased, leading to the prosperity of the cyanobacteria community and production of large oncoïds. (d) With further shallowing of the water body and excessive light intensity, the cyanobacterial mat withered and no longer formed leading to the formation of the termination bed.

The production and consumption of organic matter by photosynthetic autotrophic cyanobacteria and heterotrophic bacteria (SRB) inside the mat reached a stable balance and led to a thriving benthic microbial community. The increase in metabolic activity of this type of microbial

mat suggests conditions were favourable for the development of cyanobacteria (*Girvanella*) (Riding, 2011; Xiao *et al.*, 2018). The increase in cyanobacteria increased the mineralisation mediated by microbial metabolic mechanisms (Dupraz *et al.*, 2009; Riding, 2011; Xiao *et al.*, 2018).

The oncoids produced during this period were the largest, and their morphological characteristics were best developed (Figure 12c). (4) With the further shallowing of the water body, the accommodation space further decreased (the vertical changes in sedimentary facies in Figure 2, dolomite crystal structure in Figure 5f and carbon isotope characteristics in Figure 11), the late-stage depositional setting and elevated solar radiation led to the cessation of carbonate precipitation in the benthic cyanobacterial microbial mat (Riding, 2011, 2012; Xiao *et al.*, 2018), resulting in the formation of the growth-termination surfaces (Figure 12d).

Conclusions

The marine carbonate oncoids of the Cambrian Zhangxia Formation in the Miaolingian Series at the Sandaogou section are classified into three types: Type 1, concentric laminar oncoids; Type 2, lateral growth oncoids; and Type 3, multicore oncoids. Typical calcified cyanobacterial fossils, *Girvanella*, which are closely related to the laminae, are commonly found in these oncoids. These fossils, combined with framboidal pyrite particles and nanospheres observed at the ultra-microscale, indicate that the formation of these marine carbonate oncoids was related to the metabolic activities of cyanobacteria-dominated microbial mats and heterotrophic bacteria. Here, we suggest that these *Girvanella*-bearing oncoids are a reference example for interpretation of other marine carbonate oncoids with similar morphological characteristics.

The features of the oncoïd-bearing limestone bed within the top part of the Zhangxia Formation are: (1) an increase in size of the oncoids from the bottom (~0.5 cm) to the top of the bed (~1.5 cm), (2) a growth termination surface at the top of the massive oolitic limestone, and (3) stratigraphic changes in the proportions of oncoïd types. The carbon isotopic values and dolomite contents of the oncoïd samples both increase gradually from the bottom to the top of the bed, correspond with a shallowing-upward depositional environment and suggest that the oncolitic-oolitic limestone may have formed during a forced regression process in a fourth-order sequence. The decrease in accommodation space led to an upward-shallowing marine environment that became increasingly suitable for the development of the cyanobacteria-dominated microbial mats and enlarged growth of oncoids, and led to the stratigraphic inverse grading in oncoïd size. A late-stage evaporative setting with elevated solar radiation led to the cessation of carbonate precipitation in the benthic cyanobacterial microbial mat and the formation of the growth-termination surface.

Acknowledgements

We gratefully acknowledge Professor Mingxiang Mei for the critical reviews on the earlier versions of the manuscript. The authors are also thankful to the anonymous reviewers for their valuable suggestions to improve the paper.

Disclosure statement

No potential conflict of interest was reported by the author(s).

Funding

This work was supported by the National Key R&D Program of China ([2019YFC1509102]) and the National Natural Science Foundation of China ([41941006]).

ORCID

E. Z. Xiao  <http://orcid.org/0000-0003-3338-2423>

T. Zafar  <http://orcid.org/0000-0002-5403-8982>

M. Riaz  <http://orcid.org/0000-0002-6154-3354>

K. Latif  <http://orcid.org/0000-0002-5329-9902>

References

- Baumgartner, L. K., Reid, R. P., Dupraz, C., Decho, A. W., Buckley, D. H., Spear, J. R., Przekop, K. M., & Visscher, P. T. (2006). Sulfate reducing bacteria in microbial mats: Changing paradigms, new discoveries. *Sedimentary Geology*, 185(3–4), 131–145. <https://doi.org/10.1016/j.sedgeo.2005.12.008>
- Bosak, T., Bush, J. W. M., Flynn, M. R., Liang, B. Q., Ono, S., Petroff, A. P., & Sim, M. S. (2010). Formation and stability of oxygen-rich bubbles that shape photosynthetic mats. *Geobiology*, 8(1), 45–53. <https://doi.org/10.1111/j.1472-4669.2009.00227.x>
- Bosak, T., Liang, B., Sim, M. S., & Petroff, A. P. (2009). Morphological record of oxygenic photosynthesis in conical stromatolites. *Proceedings of the National Academy of Sciences of the United States of America*, 106(27), 10939–10943. <https://doi.org/10.1073/pnas.0900885106>
- Brasier, M. D., Corfield, R. M., Derry, L. A., Rozanov, A. Y., & Zhuravlev, A. (1994). Multiple $\delta^{13}\text{C}$ excursions spanning the Cambrian explosion to the Botomian crisis in Siberia. *Geology*, 22(5), 455–455. [https://doi.org/10.1130/0091-7613\(1994\)022<0455:MCESTC2.3.CO;2](https://doi.org/10.1130/0091-7613(1994)022<0455:MCESTC2.3.CO;2)
- Chen, H., Gong, E. P., Guan, C. Q., Sun, B. L., & Zhang, Y. L. (2008). Application of the constitution of carbon, oxygen and strontium isotopes and trace elements in study of paleoenvironment of reefs. *Global Geology*, 27(2), 130–136. <https://doi.org/10.3969/j.issn.1004-5589.2008.02.003>
- Dahanayake, K. (1977). Classification of oncoids from the upper Jurassic carbonates of the French Jura. *Sedimentary Geology*, 18(4), 337–353. [https://doi.org/10.1016/0037-0738\(77\)90058-6](https://doi.org/10.1016/0037-0738(77)90058-6)
- Diaz, M. R., Eberli, G. P., Blackwelder, P. L., Phillips, B., & Swart, P. (2017). Microbially mediated organomineralization in the formation of ooids. *Geology*, 45(9), 771–774. <https://doi.org/10.1130/G39159.1>
- Dupraz, C., Reid, R. P., Braissant, O., Decho, A. W., Norman, R. S., & Visscher, P. T. (2009). Processes of carbonate precipitation in modern microbial mats. *Earth-Science Reviews*, 96(3), 141–162. <https://doi.org/10.1016/j.earscirev.2008.10.005>
- Fan, J. X., Peng, S. C., Hou, X. D., & Chen, D. Y. (2015). Official website of the International Commission on Stratigraphy and the release of the international chronostratigraphic chart (V2015/01). *Journal of Stratigraphy*, 39(2), 125–134. <https://doi.org/10.3969/j.issn.0253-4959.2015.02.001>
- Farias, M. E., Contreras, M., Rasuk, M. C., Kurth, D., Flores, M. R., Poire, D. G., Novoa, F. F., & Visscher, P. T. (2014). Characterization of bacterial diversity associated with microbial mats, gypsum evaporites and carbonate microbialites in thalassic wetlands: Tebenquiche and La Brava, Salar de Atacama, Chile. *Extremophiles: Life under Extreme Conditions*, 18(2), 311–329. <https://doi.org/10.1007/s00792-013-0617-6>

- Feng, Z. Z., Peng, Y. M., Jin, Z. K., & Bao, Z. D. (2004). *Lithofacies paleogeography of the Cambrian and Ordovician in China* (pp. 112–121). Petroleum Industry Press. (In Chinese)
- Flügel, E., & Munnecke, A. (2010). *Microfacies of carbonate rocks*. (pp. 128–129). Springer.
- Gerdes, G., Dunajtschik-Piewak, K., Riege, H., Taher, A. G., Krumbein, W. E., & Reineck, H. E. (1994). Structural diversity of biogenic carbonate particles in microbial mats. *Sedimentology*, 41(6), 1273–1294. <https://doi.org/10.1111/j.1365-3091.1994.tb01453.x>
- Gradziński, M., Tysza, J., Uchman, A., & Jach, R. (2004). Large microbial-foraminiferal oncoids from condensed Lower-Middle Jurassic deposits: A case study from the Tatra Mountains. *Poland. Palaeogeography, Palaeoclimatology, Palaeoecology*, 213(1–2), 133–151. <https://doi.org/10.1016/j.palaeo.2004.07.010>
- Guo, Q., Jin, Z. K., Zhu, X., Shi, S. T., Wang, J. J., Wang, J. Y., Li, Y., & Li, S. (2020). Characteristics and mechanism of dolomitization in the ooids of the Cambrian Zhangxia Formation. *Carbonates and Evaporites*, 35(1), 7. <https://doi.org/10.1007/s13146-019-00545-9>
- Hägele, D., Leinfelder, R., Grau, J., Burmeister, E. G., & Struck, U. (2006). Oncoids from the river Alz (Southern Germany): Tiny ecosystems in a phosphorus-limited environment. *Palaeogeography, Palaeoclimatology, Palaeoecology*, 237(2–4), 378–395. <https://doi.org/10.1016/j.palaeo.2005.12.016>
- Han, Z. Z., Zhang, X. L., Chi, N. J., Han, M., Woo, J., Lee, H. S., & Chen, J. T. (2015). Cambrian oncoids and other microbial-related grains on the North China Platform. *Carbonates and Evaporites*, 30(4), 373–386. <https://doi.org/10.1007/s13146-014-0209-2>
- Hag, B. U., & Schutter, S. R. (2008). A chronology of Paleozoic sea-level changes. *Science*, 322(5898), 64–68. <https://doi.org/10.1126/science.1161648>
- Hoffman, P. F., Kaufman, A. J., Halverson, G. P., & Schrag, D. P. (1998). A Neoproterozoic Snowball Earth. *Science*, 281(5381), 1342–1346. <https://doi.org/10.1126/science.281.5381.1342>
- Horacek, M., Brandner, R., & Abart, R. (2007). Carbon isotope record of the P/T boundary and the Lower Triassic in the Southern Alps: Evidence for rapid changes in storage of organic carbon. *Palaeogeography, Palaeoclimatology, Palaeoecology*, 252(1–2), 347–354. <https://doi.org/10.1016/j.palaeo.2006.11.049>
- Hough, M. L., Shields, G. A., Evins, L. Z., Strauss, H., Henderson, R. A., & Mackenzie, S. (2006). A major sulphur isotope event at c. 510 Ma: A possible anoxia-extinction-volcanism connection during the Early-Middle Cambrian transition? *Terra Nova*, 18(4), 257–263. <https://doi.org/10.1111/j.1365-3121.2006.00687.x>
- Ishikawa, T., Ueno, Y., Shu, D., Li, Y., Han, J., Guo, J. F., Yoshida, N., Maruyama, S., & Komiya, T. (2014). The $\delta^{13}\text{C}$ excursions spanning the Cambrian explosion to the Canglangpuian mass extinction in the Three Gorges area, South China. *Gondwana Research*, 25(3), 1045–1056. <https://doi.org/10.1016/j.gr.2013.03.010>
- Jones, B. (1992). Void-filling deposits in karst terrains of isolated oceanic islands: A case study from Tertiary carbonates of the Cayman Islands. *Sedimentology*, 39(5), 857–876. <https://doi.org/10.1111/j.1365-3091.1992.tb02157.x>
- Jones, B. (2011). Biogenicity of terrestrial oncoids formed in soil pockets, Cayman Brac. *Sedimentary Geology*, 236(1–2), 95–108. <https://doi.org/10.1016/j.sedgeo.2010.12.009>
- Jones, B., & Renaut, R. W. (1997). Formation of silica oncoids around geysers and hot springs at El Tatio, Chile. *Sedimentology*, 44(2), 287–304. <https://doi.org/10.1111/j.1365-3091.1997.tb01525.x>
- Jones, B., & Renaut, R. W. (2010). Impact of seasonal changes on the formation and accumulation of soft siliceous sediments on the discharge apron of Geysir, Iceland. *Journal of Sedimentary Research*, 80(1), 17–35. <https://doi.org/10.2110/jr.2010.008>
- Jones, B., Renaut, R. W., & Konhauser, K. O. (2005). Genesis of large siliceous stromatolites at Frying Pan Lake, Waimangu geothermal field, North Island, New Zealand. *Sedimentology*, 52(6), 1229–1252. <https://doi.org/10.1111/j.1365-3091.2005.00739.x>
- Kaufman, A. J., & Knoll, A. H. (1995). Neoproterozoic variations in the C-isotopic composition of seawater: Stratigraphic and biogeochemical implications. *Precambrian Research*, 73(1–4), 27–49. [https://doi.org/10.1016/0301-9268\(94\)00070-8](https://doi.org/10.1016/0301-9268(94)00070-8)
- Kiessling, W. (2009). Geologic and biologic controls on the evolution of reefs. *Annual Review of Ecology, Evolution, and Systematics*, 40(1), 173–192. <https://doi.org/10.1146/annurev.ecolsys.110308.120251>
- Kimura, H., & Watanabe, Y. (2001). Oceanic anoxia at the Precambrian-Cambrian boundary. *Geology*, 29(11), 995–998. [https://doi.org/10.1130/0091-7613\(2001\)029<0995:OAAATPC>2.0.CO;2](https://doi.org/10.1130/0091-7613(2001)029<0995:OAAATPC>2.0.CO;2)
- Kouchinsky, A., Bengtson, S., Gallet, Y., Korovnikov, I., Pavlov, V., Runnegar, B., Shields, G., Veizer, J., Young, E., & Ziegler, K. (2008). The SPICE carbon isotope excursion in Siberia: A combined study of the upper Middle Cambrian-lowermost Ordovician Kulyumbe River section, northwestern Siberian Platform. *Geological Magazine*, 145(5), 609–622. <https://doi.org/10.1017/S0016756808004913>
- Krumbein, W. E., & Cohen, Y. (1977). *Primary Production, Mat Formation and Lithification: Contribution of Oxygenic and Facultative Anoxygenic Cyanobacteria* (pp. 37–56). Springer-Verlag.
- Kump, L. R., & Arthur, M. A. (1999). Interpreting carbon-isotope excursions: Carbonates and organic matter. *Chemical Geology*, 161(1–3), 181–198. [https://doi.org/10.1016/S0009-2541\(99\)00086-8](https://doi.org/10.1016/S0009-2541(99)00086-8)
- Latif, K., Xiao, E. Z., Riaz, M., & Hussein, A. A. A. (2019). Calcified cyanobacteria fossils from the leiolitic bioherm in the Furongian Changshan Formation, Datong (North China Platform). *Carbonates and Evaporites*, 34(3), 825–843. <https://doi.org/10.1007/s13146-018-0472-8>
- Latif, K., Xiao, E. Z., Riaz, M., Wang, L., Khan, M. Y., Hussein, A. A., & Khan, M. U. (2018). Sequence stratigraphy, sea-level changes and depositional systems in the Cambrian of the North China Platform: A case study of Kouquan section, Shanxi Province, China. *Journal Himalayan Earth Sciences*, 51(1), 1–16.
- Li, X. Z., Guan, S. R., Xie, Q. B., & Wang, Z. C. (2000). The oncoids genesis in the Middle Member of the Guanzhuang Formation of Eocene in Pingyi Basin. *Acta Petrologica Sinica*, 16(2), 261–268. <https://doi.org/10.3969/j.issn.1000-0569.2000.02.016>
- Liu, W., & Zhang, X. L. (2012). *Girvanella*-coated grains from Cambrian oolitic limestone. *Facies*, 58(4), 779–787. <https://doi.org/10.1007/s10347-012-0294-4>
- Liu, W., & Zhang, X. L. (2015). Calcified biofilms from Cambrian oolitic limestones in China. *Acta Geologica Sinica*, 89(1), 70–76. <https://doi.org/10.1111/1755-6724.12395>
- Mei, M. X. (2007). Revised classification of microbial carbonates: Complementing the classification of limestones. *Earth Science Frontiers*, 14(5), 222–234. [https://doi.org/10.1016/S1872-5791\(07\)60044-X](https://doi.org/10.1016/S1872-5791(07)60044-X)
- Mei, M. X., & Gao, J. H. (2015). Photosynthesis signals represented by the stromatolitic formation: An excellent revelation from the study on morphology of conical stromatolites. *Geoscience. In Chinese with English Abstract*, 6, 1328–1338. <https://doi.org/10.3969/j.issn.1000-8527.2015.06.007>
- Montaeg, I. P., Osleger, D. A., & Banner, J. L. (2000). Evolution of the Sr and C isotope composition of Cambrian Oceans. *GSA Today*, 10(5), 1–5. <https://doi.org/10.3969/j.issn.1000-8527.2015.06.007>
- Peng, S. C., Babcock, L., & Cooper, R. A. (2012). *The Cambrian Period: Geologic Time Scale* (pp. 437–488). Columbia University Press.
- Peryt, T. M. (1983). Classification of coated grains. In T. M. Peryt (Ed.), *Coated Grains* (pp. 3–6). Springer.
- Peters, S. E., & Gaines, R. R. (2012). Formation of the ‘Great Unconformity’ as a trigger for the Cambrian explosion. *Nature*, 484(7394), 363–366. <https://doi.org/10.1038/nature10969>
- Pratt, B. R. (2001). Calcification of cyanobacterial filaments: *Girvanella* and the origin of lower Paleozoic lime mud. *Geology*, 29(9), 763–766. [https://doi.org/10.1130/0091-7613\(2001\)029<0763:COFCFGA>2.0.CO;2](https://doi.org/10.1130/0091-7613(2001)029<0763:COFCFGA>2.0.CO;2)
- Pratt, B. R., & Bordonar, O. L. (2007). Tsunamis in a stormy sea: Middle Cambrian inner-shelf limestones of western Argentina. *Journal of Sedimentary Research*, 77(4), 256–262. <https://doi.org/10.2110/jr.2007.032>

- Pruss, S. B., Finnegan, S., Fischer, W. W., & Knoll, A. H. (2010). Carbonates in skeleton-poor seas: New insights from Cambrian and Ordovician strata of Laurentia. *PALAIOS*, 25(2), 73–84. <https://doi.org/10.2110/palo.2009.p09-101r>
- Qi, Y. A., Chai, S., Zhang, X. Y., & Dai, M. Y. (2016). Oncoids and their depositional features from the second member of Mantou Formation (Cambrian Series 3), Weihui area, Henan Province. *China Science Paper*, 21(11), 2416–2421. <https://doi.org/10.13278/j.cnki.jjuese.201702107>
- Reolid, M., & Nieto, L. M. (2010). Jurassic Fe-Mn macro-oncoids from pelagic swells of the External Subbetic (Spain): Evidences of microbial origin. *Geologica Acta*, 8(2), 151–168. <https://doi.org/10.1344/105.000001525>
- Riaz, M., Latif, K., Zafar, T., Xiao, E. Z., Ghazi, S., Wang, L., & Hussein, A. A. A. (2019). Assessment of Cambrian sequence stratigraphic style of the North China Platform exposed in Wuhai division. *Inner Mongolia. Himalayan Geology*, 40(1), 92–102.
- Riaz, M., Xiao, E. Z., Latif, K., & Zafar, T. (2019). Sequence-stratigraphic position of oolitic bank of Cambrian in North China Platform: Example from the Kelan Section of Shanxi Province. *Arabian Journal for Science and Engineering*, 44(1), 391–407. <https://doi.org/10.1007/s13369-018-3403-z>
- Riding, R. (2006). Microbial carbonate abundance compared with fluctuations in metazoan diversity over geological time. *Sedimentary Geology*, 185(3–4), 229–238. <https://doi.org/10.1016/j.sedgeo.2005.12.015>
- Riding, R. (2011). Calcified cyanobacteria. In J. Reitner & V. Thiel (Eds.), *Encyclopedia of Geobiology: Encyclopedia of Earth Science Series* (pp. 211–223). Springer.
- Riding, R. (2012). Geochemistry. A hard life for cyanobacteria. *Science*, 336(6080), 427–428. <https://doi.org/10.1126/science.1221055>
- Riding, R., & Liang, L. (2005). Geobiology of microbial carbonates: Metazoan and seawater saturation state influences on secular trends during the Phanerozoic. *Palaeogeography, Palaeoclimatology, Palaeoecology*, 219(1–2), 101–115. <https://doi.org/10.1016/j.palaeo.2004.11.018>
- Roberts, J. A., Kenward, P. A., Fowle, D. A., Goldstein, R. H., Gonzalez, L. A., & Moore, D. S. (2013). Surface chemistry allows for abiotic precipitation of dolomite at low temperature. *Proceedings of the National Academy of Sciences*, 110(36), 14540–14514 545. <https://doi.org/10.1073/pnas.1305403110>
- Schaefer, M. O., Gutzmer, J., & Beukes, N. J. (2001). Late Paleoproterozoic Mn-rich oncoids: Earliest evidence for microbially mediated Mn precipitation. *Geology*, 29(9), 835–838. [https://doi.org/10.1130/0091-7613\(2001\)029<0835:LPMROE>2.0.CO;2](https://doi.org/10.1130/0091-7613(2001)029<0835:LPMROE>2.0.CO;2)
- Schlager, W. (1999). Type 3 sequence boundaries. In P. M. Harris, A. H. Saller, & J. A. Simo (Eds.), *Carbonate Sequence Stratigraphy: Application to Reservoirs, Outcrops and Models* (pp. 35–46). SEPM Special Publication. 63.
- Schlager, W., & Warrlich, G. (2009). Record of sea-level fall in tropical carbonates. *Basin Research*, 21(2), 209–224. <https://doi.org/10.1111/j.1365-2117.2008.00383.x>
- Shapiro, R. S., Fricke, H. C., & Fox, K. (2009). Dinosaur-bearing oncoids from ephemeral lakes of the Lower Cretaceous Cedar Mountain Formation, Utah. *PALAIOS*, 24(1), 51–58. <https://doi.org/10.2110/palo.2008.p08-013r>
- Shi, G. R., & Chen, Z. Q. (2006). Lower Permian oncoids from South China: Implications for equatorial sea-level responses to late Paleozoic Gondwanan glaciation. *Journal of Asian Earth Sciences*, 26(3–4), 424–436. <https://doi.org/10.1016/j.jseaes.2005.10.009>
- Tucker, M. E., & Wright, M. E. (1990). *Carbonate Sedimentology*, p. 482. Wiley-Blackwell.
- Védrine, S. (2008). Co-occurrence of the foraminifer *Mohlerina basilienensis* with *Bacinella-Lithocodium* oncoids: Palaeoenvironmental and palaeoecological implications (Late Oxfordian, Swiss Jura). *Journal of Micropalaeontology*, 27(1), 35–44. <https://doi.org/10.1144/jm.27.1.35>
- Védrine, S., Andre, S., & Hug, W. (2007). Oncoid growth and distribution controlled by sea-level fluctuations and climate (late Oxfordian, Swiss Jura Mountains). *Facies*, 53(4), 535–552. <https://doi.org/10.1007/s10347-007-0114-4>
- Vinogradov, V. I. (2008). Carbon and oxygen isotopic composition of the Vendian-Cambrian carbonate rocks and paleoecological reconstructions. *Lithology and Mineral Resources. Lithology and Mineral Resources*, 43(1), 44–57. <https://doi.org/10.1134/S0024490208010045>
- Wang, H., & Xiao, E. Z. (2018). Oncolites in Cambrian Series 3 at Diaquan section in Lingqiu, Shanxi. *Journal of Northeast Petroleum University*, 42(5), 44–53. <https://doi.org/10.3969/j.issn.2095-4107.2018.05.005>
- Wang, H. Z., Shi, X. Y., Wang, X. L., & Yin, H. F. (2000). *Research on the sequence stratigraphy of China* (p. 457). Guangdong Science and Technology Press. (in Chinese)
- Wilmeth, D. T., Corsetti, F. A., Bisenic, N., Dornbos, S. Q., Oji, T., & Gonchigdorj, S. (2015). Punctuated growth of microbial cones within early Cambrian oncoids. *PALAIOS*, 30(12), 836–845. <https://doi.org/10.2110/palo.2015.014>
- Xiao, E. Z., Latif, K., Riaz, M., Qin, Y. L., & Wang, H. (2018). Calcified microorganisms bloom in Furongian of the North China Platform: Evidence from microbialitic-bioherm in Qijiayu Section. *Open Geosciences*, 10(1), 250–260. <https://doi.org/10.1515/geo-2018-0019>
- Xiao, E. Z., Mei, M. X., Jiang, S., & Zafar, T. (2020). Morphology and features of Cambrian oncoids and responses to palaeogeography of the North China Platform. *Journal of Palaeogeography*, 9(1), 1–18. <https://doi.org/10.1186/s42501-020-0055-1>
- Xiao, E. Z., Qin, Y. L., Riaz, M., Latif, K., Yao, L., & Wang, H. (2017). Sequence stratigraphy division of Cambrian in the northeast area of Lvliang mountain: A case study of the Cangerhui section in Wenshui City. *Journal of Northeast Petroleum University*, 41(5), 1–19. <https://doi.org/10.3969/j.issn.2095-4107.2017.05.005>
- Xiao, E. Z., Sui, M. Y., Latif, K., & Riaz, M. (2017). Study advances and existed problem for the forming mechanism of the microbial dolomite. *Petroleum Geology & Oilfield Development in Daqing*, 36(6), 16–26. <https://doi.org/10.3969/J.ISSN.1000-3754.2017.02.004>
- Xiao, E. Z., Sui, M. Y., Qin, Y. L., Latif, K., & Riaz, M. (2017). Sequence-stratigraphy division of Cambrian in Qijiayu section. *Petroleum Geology & Oilfield Development in Daqing*, 36(6), 16–26. <https://doi.org/10.19597/J.ISSN.1000-3754.2017.01.011>
- Xiao, E. Z., Wang, H., Qin, Y. L., Latif, K., & Riaz, M. (2020). Sedimentary fabrics and environmental characteristics of leiolite in Cambrian: A case study from Changshan Formation in Laiyuan City, Hebei Province. *Acta Sedimentologica Sinica*, 38(1), 76–90. <https://doi.org/10.14027/j.issn.1000-0550.2019.025>
- Xiao, E. Z., Zafar, T., Latif, K., Riaz, M., & Lu, Y. (2020). Geochemical and petrographic analyses of the Cambrian oncoids of the North China Platform: Implications for their paleogeography and paleoenvironment. *Arabian Journal for Science and Engineering*, 45(1), 307–325. <https://doi.org/10.1007/s13369-019-04146-5>
- Yang, R., Fan, A., & Han, Z. Z. (2011). Status and prospect of studies on oncoïd. *Advances in Earth Science*, 26(5), 465–474. <https://doi.org/10.11867/j.issn.1001-8166.2011.05.0465>
- Zeng, Y. F., Zhang, J. Q., Lin, W. Q., & Ye, Y. P. (1983). Types and environmental significance of oncoids from Yongxian Formation of the Upper Devonian in Siding, Guangxi. *Acta Sedimentologica Sinica*, 7(1), 42–49.
- Zhang, W. H., Shi, X. Y., Tang, D. J., & Wang, X. (2014). Mass-occurrence of oncoids in the early-middle Cambrian transition at western margin of North China Platform: A response of microbial community to shallow marine anoxia. *Journal of Palaeogeography*, 16(3), 305–318. <https://doi.org/10.7605/gdxb.2014.03.027>
- Zhang, X. Y., Qi, Y. A., Dai, M. Y., & Chai, S. (2015). Coupling variation of oncoids and trace fossils in the Zhangxia Formation (Cambrian Miaolingian Series), Dengfeng, western Henan Province. *Acta Micropalaeontologica Sinica*, 32(2), 184–193. <https://doi.org/10.16087/j.cnki.1000-0674.2015.02.007>

- Zhou, G., Zheng, R., & Zhao, G. (2017). Characteristics, origin and geological significance of oncoids of Givetian (Middle Devonian) in Ganxi Area, northwestern Sichuan. *Journal of Jilin University*, 47(2), 405–417. <https://doi.org/10.13278/j.cnki.jjuese.201702107>
- Zhu, M-Y., Zhang, J-M., Li, G-X., & Yang, A-H. (2004). Evolution of C isotopes in the Cambrian of China: Implications for Cambrian subdivision and trilobite mass extinctions. *Geobios*, 37(2), 287–301. <https://doi.org/10.1016/j.geobios.2003.06.001>
- Zhu, T. T., Lin, Y. C., Lu, X. C., & Dittrich, M. (2018). Assessment of cyanobacterial species for carbonate precipitation on mortar surface under different conditions. *Ecological Engineering*, 120, 154–163. <https://doi.org/10.1016/j.ecoleng.2018.05.038>